

Numerical simulation of a 2D squirmer in a rectangular microchannel

by

Harshita Tiwari and Sanket Biswas
(GCT/1940097 and GCT/1940108)

under the supervision of

Dr. Kamlesh Kumari



Department of Chemical Engineering
Sant Longowal Institute of Engineering and Technology (SLIET)

Longowal, Sangrur, Punjab

May 2023

Numerical simulation of a 2D squirmer in a rectangular microchannel

by

Harshita Tiwari¹ and Sanket Biswas²
(GCT/1940097 and GCT/1940108)



under the supervision of

Dr. Kamlesh Kumari³
Professor

Department of Chemical Engineering
Sant Longowal Institute of Engineering and Technology (SLIET)

A project report submitted to the
Department of Chemical Engineering
Sant Longowal Institute of Engineering and Technology (SLIET), Longowal
in fulfillment of the
BE Hons. Project (PHCH-721) requirement for the degree of
Bachelor of Engineering Hons. (BE Hons.) in Chemical Engineering

Longowal, Sangrur, Punjab
May 2023

¹Email address: 1940097@sliet.ac.in

²Email address: 1940108@sliet.ac.in

³Email address: kamlesh213@sliet.ac.in

Abstract

This thesis explores the swimming dynamics of squirmers in both an unbounded quiescent fluid medium and a confined rectangular microchannel under Stokes flow conditions. The primary objective is to develop a self-sustainable numerical simulation framework, utilizing software such as COMSOL, OpenFOAM, or other suitable CFD simulation software, to model the dynamics of microswimmers as squirmers. The governing fluid flow equations for both bounded and unbounded domains are solved through the finite element method (FEM) using appropriate finite elements and mesh sizes. The equations of motion (EOMs) are numerically solved using iterative methods such as Euler's method. The simulations are performed for different swimming modes and self-propulsion strengths of the squirmers, subject to appropriate initial conditions.

In the rectangular microchannel, the simulation results reveal that the geometry of the channel significantly influences the swimming dynamics of the squirmers. For instance, the confinement of the channel walls can lead to changes in the propulsion mechanism of the micro-swimmers. The velocity fields induced by the squirmers display significant variations over time, reflecting the impact of the self-propulsion strength and the hydrodynamic and non-hydrodynamic interactions with the channel's top and bottom walls.

The computational simulations provide insights into the swimming dynamics and navigation strategies of squirmers in various domains, which can have implications for propulsion efficiency, navigation strategies, and response to different confinement conditions. The results obtained from the simulations can contribute to the development of better microswimmers for drug delivery and other applications.

Overall, this research provides a comprehensive investigation of the swimming dynamics of squirmers and highlights the importance of simulations in understanding the behavior of micro-swimmers in different domains.

Examining Committee Membership

The following served on the Examining Committee for this report. The decision of the Examining Committee is by majority vote.

Internal Examiners:	Dr. Pushpa Jha Professor and HoD, Dept. of Chemical Engineering, SLIET Longowal Dr. Sandeep Mohan Ahuja Professor, Department of Chemical Engineering, SLIET Longowal
Project Supervisor:	Dr. Kamlesh Kumari Professor, Department of Chemical Engineering, SLIET Longowal

Authors' Declaration

We declare that the contents of this report are original and have been produced solely by us. We further attest that, to the best of our knowledge and belief, it does not contain any previously published material or work written by another person, nor does it consist of material that has been accepted for the award of any other degree or diploma from this university or any other institute of higher learning, unless we have appropriately acknowledged and referenced such material in the text.

Harshita Tiwari

Ms. Harshita Tiwari
(GCT/1940097)

.....
14/05/2023

Date

Sanket Biswas.

Mr. Sanket Biswas
(GCT/1940108)

.....
14/05/2023

Date

Acknowledgements

We would like to express our gratitude to all those who have supported and guided us throughout this project. First and foremost, we extend our deepest thanks to our esteemed project supervisor Dr. Kamlesh Kumari for granting us the opportunity to work on a fascinating project in active matter and microfluidics. Her diligent guidance on numerous scientific questions served as hooks in our research, and we are grateful for her prompt responses to our queries and questions. We commend her patience and encouragement as she challenged us to think critically and provided regular constructive feedback on our weekly project reports. Her feedback has been a catalyst for our personal and professional growth, and we feel honored to have had her as our supervisor.

We also acknowledge and extend our sincere appreciation to Prof. Shubhadeep Mandal and Prof. Aloke Kumar for their invaluable support and dedication throughout our project. Their expertise and guidance have been instrumental in shaping our understanding of our research work and its potential applications in various fields. We are extremely grateful for their invaluable support and unconventional thinking, which enabled us to establish a strong rapport with them based on open and trusting communication.

We also express our gratitude to the graduate students and project assistants of Complex & Biological Fluids Lab (Prof. Shubhadeep Mandal's Lab) and Prof. Aloke Kumar's Lab at IISc for their immense support and friendship during the completion of this work. Their selfless mentorship and guidance have been instrumental in our research progress, and we are indebted to them.

Finally, we would like to acknowledge and thank our family and friends for their constant and unwavering encouragement throughout our journey as aspiring researchers. Their unwavering support has been a constant source of inspiration and motivation, and we owe them a debt of gratitude for their role in our success. We will always cherish their support and encouragement.

Certificate

This is to certify that, Ms. Harshita Tiwari (GCT/1940097) and Mr. Sanket Biswas (GCT/1940108), both of whom are pursuing a Bachelor of Engineering Hons. (BE Hons.) in Chemical Engineering from Sant Longowal Institute of Engineering and Technology (SLIET) have successfully completed their BE Hons. Project (Jan. '23 to Jun. '23) on the *Numerical simulation of a 2D squirmer in a rectangular microchannel* at the Department of Chemical Engineering, Sant Longowal Institute of Engineering and Technology (SLIET), Longowal. They have successfully presented their work at the BE Hons. Project Seminar and have also submitted a hard copy and a soft copy of this report for further reference and record. The final evaluation was done offline at the Department of Chemical Engineering of SLIET by a select and experienced group of faculties of the department.

.....
Dr. Kamlesh Kumari
(Project Supervisor)

.....
Date

Table of Contents

1	Introduction	1
1.1	Background and motivation	1
1.2	Overview of our research	3
1.3	Mapping of COs and POs	3
2	Swimming dynamics in an infinite quiescent fluid medium	4
2.1	Modelling a microswimmer in an unbounded quiescent fluid medium	4
2.1.1	Squirmer model	4
2.1.2	Domain specifications	7
2.2	Numerical method	10
2.2.1	Squirmer dynamics	10
2.2.2	Non-dimensionalisation	12
2.2.3	Simulation parameters for the co-moving frame	13
2.3	Results and discussion	15
2.3.1	Time evolution of the squirmer's velocity magnitude	15
2.3.2	Variation of the x -component of squirmer's velocity with orientation angle θ	17
2.3.3	Variation of the y -component of squirmer's velocity with orientation angle θ	19
2.3.4	Variation of the squirmer's rotational speed with orientation angle θ	21
2.3.5	Velocity profile	23

3 Swimming dynamics in a rectangular microchannel with quiescent fluid	25
3.1 Modelling a microswimmer in a rectangular microchannel with stationary fluid	25
3.1.1 Squirmer model	25
3.1.2 Domain specifications	25
3.2 Numerical method	28
3.2.1 Squirmer dynamics	28
3.2.2 Non-dimensionalisation	30
3.2.3 Wall-induced hydrodynamic interactions	30
3.2.4 Wall induced non-hydrodynamic interactions	31
3.2.5 Simulation parameters for the x -moving frame	32
3.3 Results and discussion	33
3.3.1 Confinement induced trajectories	33
3.3.2 Time evolution of the squirmer's velocity magnitude	34
3.3.3 Variation of the x and y -component of squirmer's velocity with orientation angle θ	35
3.3.4 Velocity profile	38
4 Appendix	40
References	41

Chapter 1

Introduction

This research paper is structured around the investigation of the swimming dynamics of squirmers in unbonded and confined domains under stokes flow conditions. This study is divided into three chapters to comprehensively explore the swimming behavior of squirmers, with the initial chapter providing an introduction to the topic, outlining the motivation and goals of our research. The second chapter deals with the swimming dynamics of squirmers in an unbounded domain, where the squirmer is free to move and explore a limitless space. The third chapter focuses on the locomotion of squirmers in a confined domain, where the fluid environment is constrained by physical boundaries, such as narrow channels or porous media. The investigation of these phenomena contributes to the understanding of the locomotion of sperm cells in the female reproductive tract, targeted drug delivery, and biofilm formation.

This chapter is divided into three main sections, namely, background and motivation, overview of our research, and mapping of COs and POs, that aim to introduce and contextualize our study.

1.1 Background and motivation

In the past few decades, the swimming dynamics of squirmers have gained significant attention due to their involvement in various survival mechanisms [1]. These particles derive energy from their surrounding environment and efficiently convert it into directed motion [2]. These microscopic particles fall into the Stokesian realm. In this regime, their dynamics are dominated by the viscous force of the surrounding fluid medium rather than the advective inertial forces.

Microswimmers often experience hydrodynamic and non-hydrodynamic interactions [3] when they are confined within walls or boundaries. These interactions hold significant implications in various scenarios [4, 5], and can modify the translational and angular velocities of microswimmers, leading to distinct trajectories within confined spaces compared to the bulk environment. Understanding these phenomena is crucial not only for comprehending sperm locomotion in the female reproductive tract [6] but also for the development of artificial microswimmers with applications in drug delivery and sensing [7].

[8] discovered significant variations in the locomotion of pusher and puller squirmers when considering fluid inertia. The researchers observed that pushers exhibit a monotonically increasing swimming speed as the Reynolds number (Re) rises. On the other hand, pullers display a non-monotonic relationship between swimming speed and Re .

[9] obtained the trajectories of a micro-swimmer, confined between two parallel walls, by using the lattice Boltzmann method (LBM). The researchers then proceeded to examine and contrast the trajectories influenced by confinement with those in an unbounded environment. Their findings revealed that the hydrodynamic interactions between the squirmer and the wall can induce either attraction or repulsion, as well as reorientation, ultimately leading to a hydrodynamic collision with the wall. Additionally, they introduced the concept of wall potential, which triggered an infinite repulsive force when the swimmer approached the wall within a specific cut-off distance.

A recent simulation study investigated the interaction of circular squirmers in a two-dimensional channel under the influence of gravity and finite fluid inertia [10]. The study observed that pullers, characterized by their forward propulsion, tend to attract each other and eventually make contact. This behavior is attributed to the formation of low-pressure regions between them. On the other hand, pushers, which exhibit backward propulsion, maintain a distance from each other and do not come into contact even as the separation between them increases. Furthermore, they introduce a control parameter, representing the ratio of the self-propelling strength to the sedimentation strength of squirmers.

By simulating the behavior of confined micro-swimmers, researchers can gain insights into their propulsion efficiency, navigation strategies, and response to different confinement conditions. These models can also be used to optimize the design of artificial micro-robots or study biological microorganisms' behavior in complex environments.

Therefore, in this study, we investigate the behavior of squirmers (pushers and pullers) using the finite element method in COMSOL Multiphysics.

1.2 Overview of our research

In Chapter 2, we delve into the swimming dynamics of squirmers in a fluid domain without boundaries. Through the utilization of finite element method and computational simulations using COMSOL Multiphysics, we analyze the various swimming strategies employed by squirmers and examine their effects.

In Chapter 3, our research focuses on investigating the locomotion of squirmers within a confined fluid domain. This chapter specifically explores how geometric confinement influences the motion and behavior of squirmers, taking into account both hydrodynamic and non-hydrodynamic interactions. To gain insights into the swimming dynamics and navigation strategies of squirmers in confined domains, we employed the finite element method and performed numerical simulations using COMSOL Multiphysics.

1.3 Mapping of COs and POs

After conducting a comprehensive analysis of the research background, motivation, problem statements, achieved objectives, scope and potential applications of our study, as well as possibilities for future research, we have concluded that our work is consistent with the predefined program objectives (POs) and course objectives (COs), which are detailed below:

POs & COs	PO1	PO2	PO3	PO4	PO5	PO6	PO7	PO8	PO9	PO10	PO11	PO12	PSO1	PSO2
CO1	S	S	W	S	S	M	S	S	S	S	M	M	M	S
CO2	S	S	S	S	S	S	M	S	S	S	M	M	M	S
CO3	S	M	M	S	S	M	S	S	S	S	M	M	M	S

Chapter 2

Swimming dynamics in an infinite quiescent fluid medium

2.1 Modelling a microswimmer in an unbounded quiescent fluid medium

2.1.1 Squirmer model

In this research, we employed the *squirmer model* proposed by [11] and [12] to simulate the motion of a microswimmer in an unbounded or infinite quiescent fluid medium. According to [12], a squirmer is defined as a circular rigid particle having a prescribed *surface slip velocity* \mathbf{u}^S , which can be expressed as an infinite series expansion of the radial and polar components, as follows:

$$\mathbf{u}^S(\mathbf{x}_s) = \sum_{n=0}^{\infty} A_n \cos(n\theta) \hat{\mathbf{e}}_r + \sum_{n=0}^{\infty} B_n \sin(n\theta) \hat{\mathbf{e}}_{\theta}. \quad (2.1)$$

Here, $\hat{\mathbf{e}}_r$ and $\hat{\mathbf{e}}_{\theta}$ denote the radial and polar unit vectors, respectively, and A_n and B_n are the time-dependent *amplitudes* or *magnitudes of the nth mode*. The angle θ is defined as the angle between the arbitrary position vector¹ on the squirmer surface, $\mathbf{x}_s = (a \sin \theta, a \cos \theta)$, and the swimmer orientation unit vector $\hat{\mathbf{e}}$ in the counterclockwise direction, where a is the radius of the squirmer, as illustrated in Fig. 2.1.

¹assuming the centre of the squirmer to be the origin

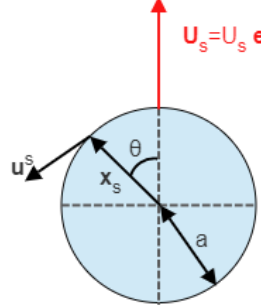


Figure 2.1: Schematic diagram illustrating a squirmer of radius a , with a surface slip velocity \mathbf{u}^s at the position vector \mathbf{x}_s . The self-propulsion velocity of the squirmer is denoted by $\mathbf{U}_s = U_s \hat{\mathbf{e}}$.

It is common to disregard the radial component of the surface slip velocity in the context of squirmers' movement problems, as per [12]. Consequently, the surface slip velocity expression simplifies to the following form in this scenario:

$$\mathbf{u}^s(\mathbf{x}_s) = \sum_{n=0}^{\infty} B_n \sin(n\theta) \hat{\mathbf{e}}_\theta. \quad (2.2)$$

Building on the above assumption, we employed a simplified squirmer model that is characterized by a second-order truncated tangential velocity, given by

$$\mathbf{u}^s(\mathbf{x}_s) = \sum_{n=0}^2 B_n \sin(n\theta) \hat{\mathbf{e}}_\theta = (B_1 \sin \theta + 2B_2 \sin \theta \cos \theta) \hat{\mathbf{e}}_\theta. \quad (2.3)$$

In an unconfined fluid, the squirmer develops a flow field [12] in lab frame of reference, given by $\mathbf{u} = u_r \hat{\mathbf{e}}_r + u_\theta \hat{\mathbf{e}}_\theta$, where

$$u_r(r, \theta) = \frac{B_1}{2} \left(\frac{a}{r} \right)^2 \cos \theta + \sum_{n=2}^{\infty} \frac{n}{2} B_n \cos(n\theta) \frac{a^{n-1}}{r^{n-1}} \left[\left(\frac{a}{r} \right)^2 - 1 \right], \quad (2.4a)$$

$$u_\theta(r, \theta) = \frac{B_1}{2} \left(\frac{a}{r} \right)^2 \sin \theta + \sum_{n=2}^{\infty} \frac{1}{2} B_n \sin(n\theta) \frac{a^{n-1}}{r^{n-1}} \left[n \left(\frac{a}{r} \right)^2 - (n-2) \right]. \quad (2.4b)$$

Thus, in an unbounded fluid, a squirmer undergoes translational motion with a velocity

$$\mathbf{U}_s = U_s \hat{\mathbf{e}} = \mathbf{u}(r = a, \theta = 0) = \frac{B_1}{2} \hat{\mathbf{e}}_r. \quad (2.5)$$

Hence, $U_s = \frac{B_1}{2}$ and only the B_1 mode determines the translational velocity. On the other hand, the coefficient B_2 describes the intensity of vorticity around the squirmer. The next modes, which capture the details of near-field fluid motion but do not contribute to swimming, are characterized by defining the parameters

$$\beta_n = \frac{B_n}{B_1}, \quad n \in \mathbb{Z}_{\geq 2}. \quad (2.6)$$

The leading order singularities associated with B_1 and B_2 are a source dipole and a force dipole [13], respectively. These two modes are often utilized in the literature [8, 14, 15], and therefore a critical parameter, $\beta_2 = B_2/B_1$, referred to as the *squirmer self-propulsion strength*, is introduced to represent three types of squirmers, namely *pushers* ($\beta < 0$), *pullers* ($\beta > 0$), and *neutral squirmers* ($\beta = 0$). Pushers such as *E. coli* and *B. subtilis* generate thrust behind their body by sucking fluid from the sides and pushing themselves through the fluid [3, 16, 17]. Pullers such as *C. reinhardtii* and *Euglena gracilis* generate thrust in front of their body by drawing fluid from the front and back and ejecting it sideways [1]. Neutral squirmers like *Volvox carteri* and *Tetrahymena thermophila* exhibit symmetric flow without vorticity and possess a source dipole flow field around their body [18]. The visual representations of the streamlines provide a direct insight into the locomotion mechanism of each type of squirmer, as depicted in Figure 2.2. The Reynolds number linked with the squirmer is denoted by Re_s in the figures.

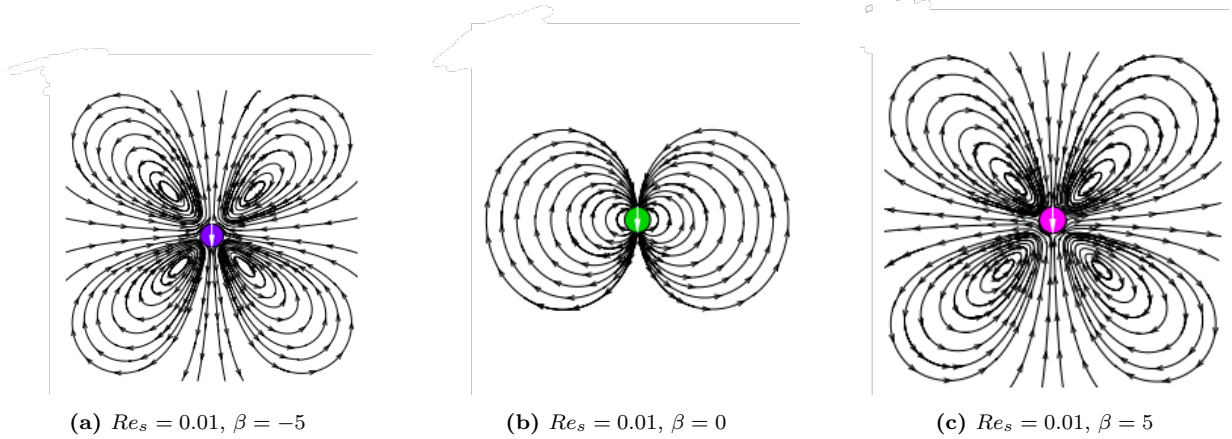


Figure 2.2

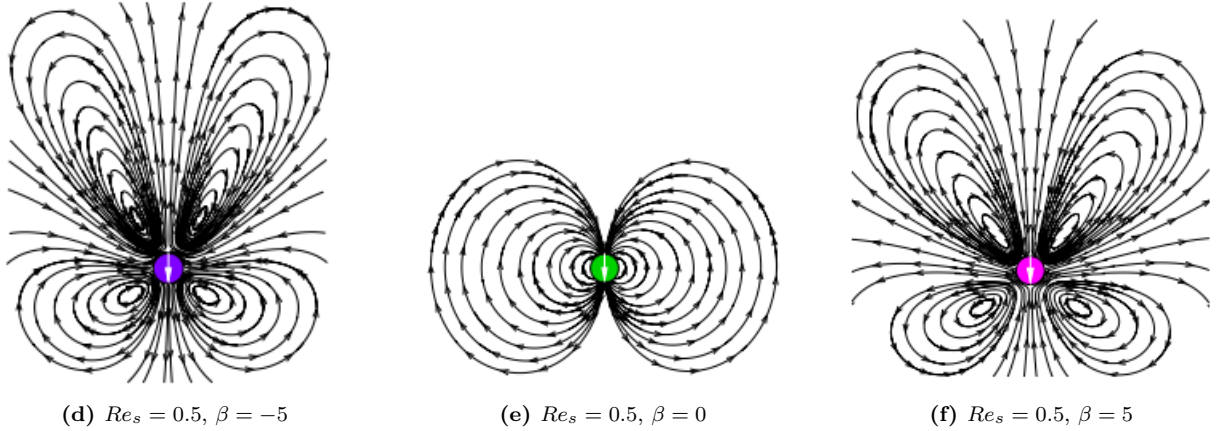


Figure 2.2: Illustration of streamlines around squirmers with varying Reynolds numbers and different propulsion strengths β . The squirmer types shown are pushers in (a) and (d), neutral squirmers in (b) and (e), and pullers in (c) and (f). The squirming axis or swimming direction of each squirmer is indicated by an arrow.

2.1.2 Domain specifications

In this study, a squirmer of radius a was considered, initially positioned at $\mathbf{x}_0 = (x_0, y_0)$ in an infinite or unbounded quiescent fluid with density ρ and dynamic viscosity μ . The Reynolds number associated with the squirmer is given by

$$Re_s = \frac{\rho U_s a}{\mu} = \frac{\rho B_1 a}{2\mu}. \quad (2.7)$$

To simulate this scenario in the laboratory frame, a two-dimensional rigid disk with a radius of a was positioned initially at $\mathbf{x}_0 = (x_0 = 50a, y_0 = 50a)$ within a square domain with side length $L = 150a$ filled with a fluid having density ρ , dynamic viscosity μ , and Reynolds number Re_s , as illustrated in Fig. 2.3. The origin is located at the bottom left corner of the domain. The fluid initial and boundary conditions are prescribed as follows:

$$\text{IC 1: } \mathbf{u}(x, y, t) = \mathbf{0} \text{ at } 0 \leq x \leq L, 0 \leq y \leq L, t = 0, \quad (2.8a)$$

$$\text{BC 1: } \mathbf{u}(x, y, t) = \mathbf{0} \text{ at } x = 0, 0 \leq y \leq L, t \geq 0, \quad (2.8b)$$

$$\text{BC 2: } \mathbf{u}(x, y, t) = \mathbf{0} \text{ at } x = L, 0 \leq y \leq L, t \geq 0, \quad (2.8c)$$

$$\text{BC 3: } \mathbf{u}(x, y, t) = \mathbf{0} \text{ at } 0 \leq x \leq L, y = 0, t \geq 0, \quad (2.8d)$$

$$\text{BC 4: } \mathbf{u}(x, y, t) = \mathbf{0} \text{ at } 0 \leq x \leq L, y = L, t \geq 0. \quad (2.8e)$$

(2.8)

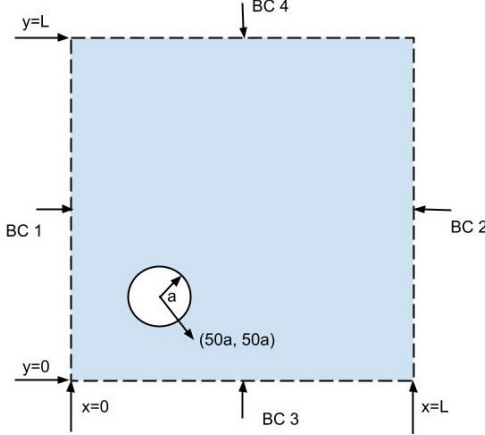


Figure 2.3: The figure illustrates the initial setup of an unbounded stationary fluid medium in the lab frame, represented by a square domain with a side length of $L = 150a$, containing a two-dimensional disk squirmer of radius a initially positioned at $\mathbf{x}_0 = (50a, 50a)$. The fluid velocity satisfies the initial and boundary conditions given in Eqn. (2.8).

The fluid dynamics around the squirmer is governed by the incompressible Navier-Stokes equations, as follows:

$$\nabla \cdot \mathbf{u} = 0, \quad (2.9a)$$

$$\rho \left(\frac{\partial \mathbf{u}}{\partial t} + \mathbf{u} \cdot \nabla \mathbf{u} \right) = -\nabla p + \mu \nabla^2 \mathbf{u}, \quad (2.9b)$$

where \mathbf{u} and p represent the velocity and pressure fields of the surrounding fluid, respectively. To solve Eqn. (2.9), the finite element method (FEM) is employed using simulation software such as COMSOL or other suitable options, as discussed in [19–21].

In simulation software, such as COMSOL, it is common to utilize a *co-moving frame* to model the motion of a microswimmer. This frame moves along with the model squirmer at the same translational velocity, while assuming zero rotational velocity for the frame.

To model the motion of the squirmer in the co-moving frame, we consider a two-dimensional non-deformable disk of radius a , initially placed at $\mathbf{x}_0 = (25a, 25a)$ inside a square domain of side length $L = 50a$. This domain is filled with a fluid of density ρ , dynamic viscosity μ , and Reynolds number Re_s , as shown in Fig. 2.4. We modify the initial and boundary

conditions for the fluid velocity as follows:

$$\text{IC 1: } \mathbf{u}(x, y, t) = -\mathbf{U}_s(t = 0) \text{ at } 0 \leq x \leq L, 0 \leq y \leq L, t = 0, \quad (2.10a)$$

$$\text{BC 1: } \mathbf{u}(x, y, t) = -\mathbf{U}_s(t) \text{ at } x = 0, 0 \leq y \leq L, t \geq 0, \quad (2.10b)$$

$$\text{BC 2: } \mathbf{u}(x, y, t) = -\mathbf{U}_s(t) \text{ at } x = L, 0 \leq y \leq L, t \geq 0, \quad (2.10c)$$

$$\text{BC 3: } \mathbf{u}(x, y, t) = -\mathbf{U}_s(t) \text{ at } 0 \leq x \leq L, y = 0, t \geq 0, \quad (2.10d)$$

$$\text{BC 4: } \mathbf{u}(x, y, t) = -\mathbf{U}_s(t) \text{ at } 0 \leq x \leq L, y = L, t \geq 0, \quad (2.10e)$$

(2.10)

where $\mathbf{U}_s(t)$ is the velocity of the squirmer at time t .

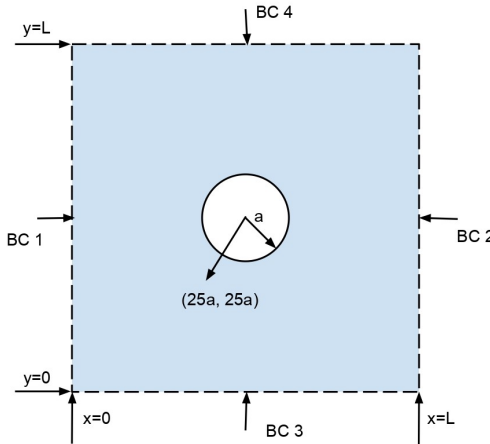


Figure 2.4: The figure illustrates the initial setup of an unbounded fluid medium in the co-moving frame, represented by a square domain with a side length of $L = 50a$, containing a two-dimensional disk squirmer of radius a initially positioned at $\mathbf{x}_0 = (25a, 25a)$. The fluid velocity satisfies the initial and boundary conditions given in Eqn. (2.10).

Note that there is no change in the fluid dynamics around the squirmer due to the frame change. Thus, the fluid dynamics around the squirmer are still governed by the incompressible Navier-Stokes equations, as described earlier in Eqn. (2.9).

2.2 Numerical method

2.2.1 Squirmer dynamics

We refer to the position of the squirmer at a given time using the position vector $\mathbf{x} = x\hat{\mathbf{e}}_x + y\hat{\mathbf{e}}_y$, while its instantaneous orientation is represented by the unit vector $\hat{\mathbf{e}} = e_x\hat{\mathbf{e}}_x + e_y\hat{\mathbf{e}}_y$, as depicted in Fig. 2.5. The squirmer's translational velocity, as previously defined, is $\mathbf{U}_s = U_x\hat{\mathbf{e}}_x + U_y\hat{\mathbf{e}}_y$, and its rotational velocity is given by $\boldsymbol{\Omega} = \Omega\hat{\mathbf{e}}_z$.

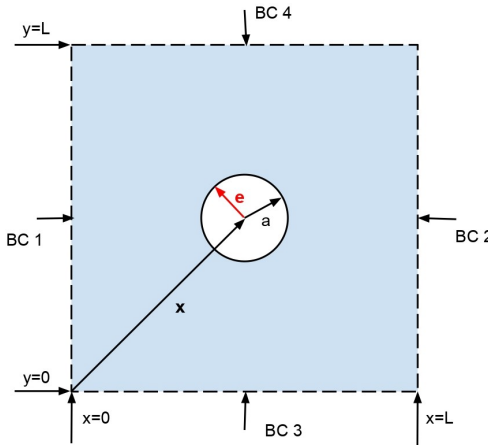


Figure 2.5

Thus, in the lab frame, at any point \mathbf{x}_s on the squirmer surface, the surface velocity \mathbf{u}_s can be expressed as follows:

$$\begin{aligned}\mathbf{u}_s(\mathbf{x}_s) &= \mathbf{u}^S(\mathbf{x}_s) + \mathbf{U}_s + \boldsymbol{\Omega} \times \mathbf{x}_s \\ &= B_1 (\sin \theta + 2\beta \sin \theta \cos \theta) \hat{\mathbf{e}}_\theta + \mathbf{U}_s + \boldsymbol{\Omega} \times \mathbf{x}_s.\end{aligned}\quad (2.11)$$

The surface velocity of the squirmer generates the fluid flow in its surrounding, and the corresponding flow field \mathbf{u} is obtained using FEM [19–21].

The governing equations of motion (EOMs) for the squirmer determine the change in its surface velocity with time, as presented below:

$$\frac{d\mathbf{x}}{dt} = \mathbf{U}, \quad \frac{d\hat{\mathbf{e}}}{dt} = \boldsymbol{\Omega} \times \hat{\mathbf{e}}, \quad (2.12a)$$

$$\frac{d\mathbf{U}}{dt} = \frac{1}{m} \iint \mathbf{f}(\mathbf{x}_s) dA, \quad (2.12b)$$

$$\frac{d\boldsymbol{\Omega}}{dt} = \frac{1}{J} \iint [\mathbf{x}_s \times \mathbf{f}(\mathbf{x}_s)] dA. \quad (2.12c)$$

(2.12)

Here, A denotes the surface of the squirmer, m is its mass, and J is its moment of inertia. The force density vector \mathbf{f} is defined for all points $\mathbf{x}_s \in A$ as follows:

$$\mathbf{f}(\mathbf{x}_s) = \boldsymbol{\tau}(\mathbf{x}_s) \cdot \hat{\mathbf{n}}(\mathbf{x}_s), \quad (2.13)$$

where $\boldsymbol{\tau}(\mathbf{x}_s)$ and $\hat{\mathbf{n}}(\mathbf{x}_s)$ represent the stress tensor and the unit normal surface vector at \mathbf{x}_s , respectively. The component-wise governing EOMs are presented below:

$$\frac{dx}{dt} = U_x, \quad \frac{dy}{dt} = U_y, \quad (2.14a)$$

$$\frac{de_x}{dt} = -\Omega e_y, \quad \frac{de_y}{dt} = \Omega e_x, \quad (2.14b)$$

$$\frac{dU_x}{dt} = \frac{1}{m} \iint_A f_x(\mathbf{x}_s) dA, \quad (2.14c)$$

$$\frac{dU_y}{dt} = \frac{1}{m} \iint_A f_y(\mathbf{x}_s) dA, \quad (2.14d)$$

$$\frac{d\Omega}{dt} = \frac{1}{J} \iint_A [x_{sx} f_y - x_{sy} f_x] dA, \quad (2.14e)$$

(2.14)

where $\mathbf{f}(\mathbf{x}_s) = f_x(\mathbf{x}_s)\hat{\mathbf{e}}_x + f_y(\mathbf{x}_s)\hat{\mathbf{e}}_y$, and $\mathbf{x}_s = x_{sx}\hat{\mathbf{e}}_x + x_{sy}\hat{\mathbf{e}}_y$, and $f_x(\mathbf{x}_s)$ and $f_y(\mathbf{x}_s)$ can be expanded as follows:

$$f_x(\mathbf{x}_s) = [\boldsymbol{\tau}(\mathbf{x}_s) \cdot \hat{\mathbf{n}}(\mathbf{x}_s)]_x, \quad f_y(\mathbf{x}_s) = [\boldsymbol{\tau}(\mathbf{x}_s) \cdot \hat{\mathbf{n}}(\mathbf{x}_s)]_y. \quad (2.15)$$

To study the motion of the squirmer in the co-moving frame, it is necessary to rewrite the squirmer surface velocity and governing EOMs accordingly. In the co-moving frame, the surface velocity is given by

$$\begin{aligned} \mathbf{u}_s(\mathbf{x}_s) &= \mathbf{u}^S(\mathbf{x}_s) + \boldsymbol{\Omega} \times \mathbf{x}_s \\ &= B_1 (\sin \theta + 2\beta \sin \theta \cos \theta) \hat{\mathbf{e}}_\theta + \boldsymbol{\Omega} \times \mathbf{x}_s. \end{aligned} \quad (2.16)$$

The component-wise EOMs in the co-moving frame are derived by applying suitable transformation to the (component-wise) EOMs in the lab frame as follows:

$$\frac{de_x}{dt} = -\Omega e_y, \quad \frac{de_y}{dt} = \Omega e_x, \quad (2.17a)$$

$$\frac{d\Omega}{dt} = \frac{1}{J} \iint_A [x_{sx} f_y - x_{sy} f_x] dA. \quad (2.17b)$$

(2.17)

Since the squirmer's velocity in the co-moving frame is always zero, only the component-wise EOMs governing the rotational velocity and acceleration are relevant, as depicted in Eqn. (2.17).

2.2.2 Non-dimensionalisation

To facilitate a dimensionless representation of the system, we scale all relevant physical quantities by appropriate scaling factors. Specifically, we scale all length variables by the radius of the squirmer a , all velocity variables by the steady-state swimming speed of the squirmer in an infinite quiescent fluid medium $U_s = B_1/2$, the time variable by a/U_s , and all force variables by mU_s^2/a . Thus, we obtain the following non-dimensional variables:

$$\tilde{x} = x/a, \quad \tilde{y} = t/a, \quad \tilde{x}_{sx} = x_{sx}/a, \quad \tilde{x}_{sy} = x_{sy}/a, \quad \tilde{t} = \frac{a}{U_s} t, \quad (2.18a)$$

$$\tilde{U}_x = U_x/U_s, \quad \tilde{U}_y = U_y/U_s, \quad \tilde{\Omega} = \frac{U_s}{a} \Omega, \quad (2.18b)$$

$$\tilde{f}_x = \frac{mU_s^2}{a} f_x, \quad \tilde{f}_y = \frac{mU_s^2}{a} f_y, \quad (2.18c)$$

(2.18)

and the following non-dimensional constants:

$$\tilde{x}_0 = x_0/a, \quad \tilde{y}_0 = y_0/a, \quad \tilde{L} = L/a. \quad (2.19)$$

Using the above non-dimensional variables, the component-wise lab frame EOMs in Eqn. (2.14) can be rewritten in a non-dimensional form, as described by the following equations:

$$\frac{d\tilde{x}}{d\tilde{t}} = \tilde{U}_x, \quad \frac{d\tilde{y}}{d\tilde{t}} = \tilde{U}_y, \quad (2.20a)$$

$$\frac{de_x}{d\tilde{t}} = -\tilde{\Omega}e_y, \quad \frac{de_y}{d\tilde{t}} = \tilde{\Omega}e_x, \quad (2.20b)$$

$$\frac{d\tilde{U}_x}{d\tilde{t}} = \iint_A \tilde{f}_x(\mathbf{x}_s/a) dA, \quad (2.20c)$$

$$\frac{d\tilde{U}_y}{d\tilde{t}} = \iint_A \tilde{f}_y(\mathbf{x}_s/a) dA, \quad (2.20d)$$

$$\frac{d\tilde{\Omega}}{d\tilde{t}} = 2 \iint_A [\tilde{x}_{sx}\tilde{f}_y - \tilde{x}_{sy}\tilde{f}_x] dA. \quad (2.20e)$$

(2.20)

The non-dimensionalized component-wise EOMs in the co-moving frame can be obtained by applying the same non-dimensionalization to the co-moving frame EOMs presented in Eqn. (2.17). They are expressed as follows:

$$\frac{de_x}{d\tilde{t}} = -\tilde{\Omega}e_y, \quad \frac{de_y}{d\tilde{t}} = \tilde{\Omega}e_x, \quad (2.21a)$$

$$\frac{d\tilde{\Omega}}{d\tilde{t}} = 2 \iint_A [\tilde{x}_{sx}\tilde{f}_y - \tilde{x}_{sy}\tilde{f}_x] dA. \quad (2.21b)$$

(2.21)

The non-dimensional component-wise EOMs in the lab frame and co-moving frame, given by Eqns. (2.20) and (2.21) respectively, are numerically solved using the Euler method, with appropriate initial conditions.

2.2.3 Simulation parameters for the co-moving frame

In this section, the simulation parameters used for the co-moving frame are presented. A domain size of 50×50 is chosen for the simulations, unless stated otherwise. The boundary conditions described in Eqn. (2.10) are applied to the four sides of the domain. To solve the Navier-Stokes equations in Eqn. (2.9) using finite element method (FEM), spatial and temporal resolutions are chosen as unity, following the standard FEM practice. The density and dynamic viscosity of the Newtonian fluid are set to $\rho = Re_s = 0.01$ and $\mu = 1$, respectively, all in lattice units.

A single squirmer with a radius of 1 lattice unit is initially placed at $(\tilde{x}_0, \tilde{y}_0) = (25, 25)$ and at an initial orientation θ_0 . An iterative procedure, such as Euler's method, is used

to calculate the squirmer's position and components of squirmer velocity using the non-dimensional governing equations of motion (EOMs) in Eqns. (2.20) and (2.21) on the steady-state flow fields obtained using FEM. The iterative procedure is continued until the magnitude of the swimming velocity, U_s , is within an error of 0.1% of the theoretical value of $B_1/2$. The time step taken for this iterative procedure is $\Delta t = 1$.

For the FEM, the mesh elements are taken to be free triangular, and the maximum size of the mesh near the squirmer's surface is set to 0.025. For the rest of the domain, the maximum size of the mesh is taken to be 1, as illustrated in Fig. 2.6.

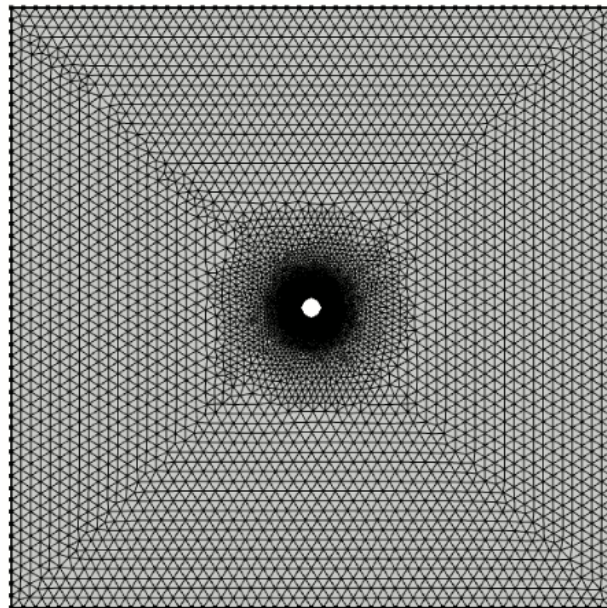


Figure 2.6: The simulation mesh employed in COMSOL for the co-moving frame has a maximum element size of 1 for the majority of the domain, with a smaller maximum size of 0.025 near the surface of the squirmer.

2.3 Results and discussion

2.3.1 Time evolution of the squirmer's velocity magnitude

Each plot in Fig. 2.7 depicts the non-dimensional velocity magnitude of the squirmer, $\tilde{U}_s = \sqrt{\tilde{U}_x^2 + \tilde{U}_y^2}$, as a function of non-dimensional time \tilde{t} , corresponding to different values of B_1 and β . The plots are organized in rows, where each row represents squirmers with a fixed value of B_1 . Within each row, the values of β are chosen to be representative of pushers ($\beta = -2$), neutral swimmers ($\beta = 0$), and pullers ($\beta = 2$). The plots reveal that the squirmer's velocity magnitude eventually reaches a steady state value of $\frac{B_1}{2}$, consistent with the theoretical value derived in Eqn. (2.5), indicating the correctness of our numerical simulation model. Furthermore, the plots indicate that the self-propulsion strength β does not significantly affect the velocity magnitude \tilde{U}_s as a function of time for a given B_1 .

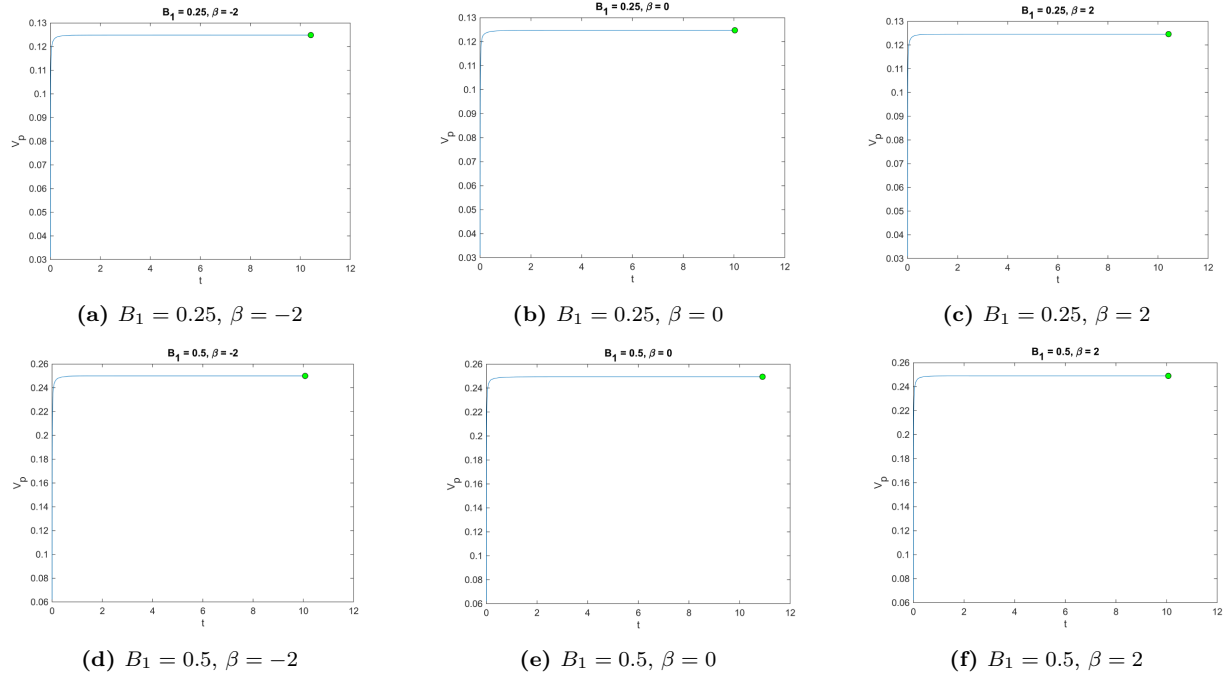


Figure 2.7

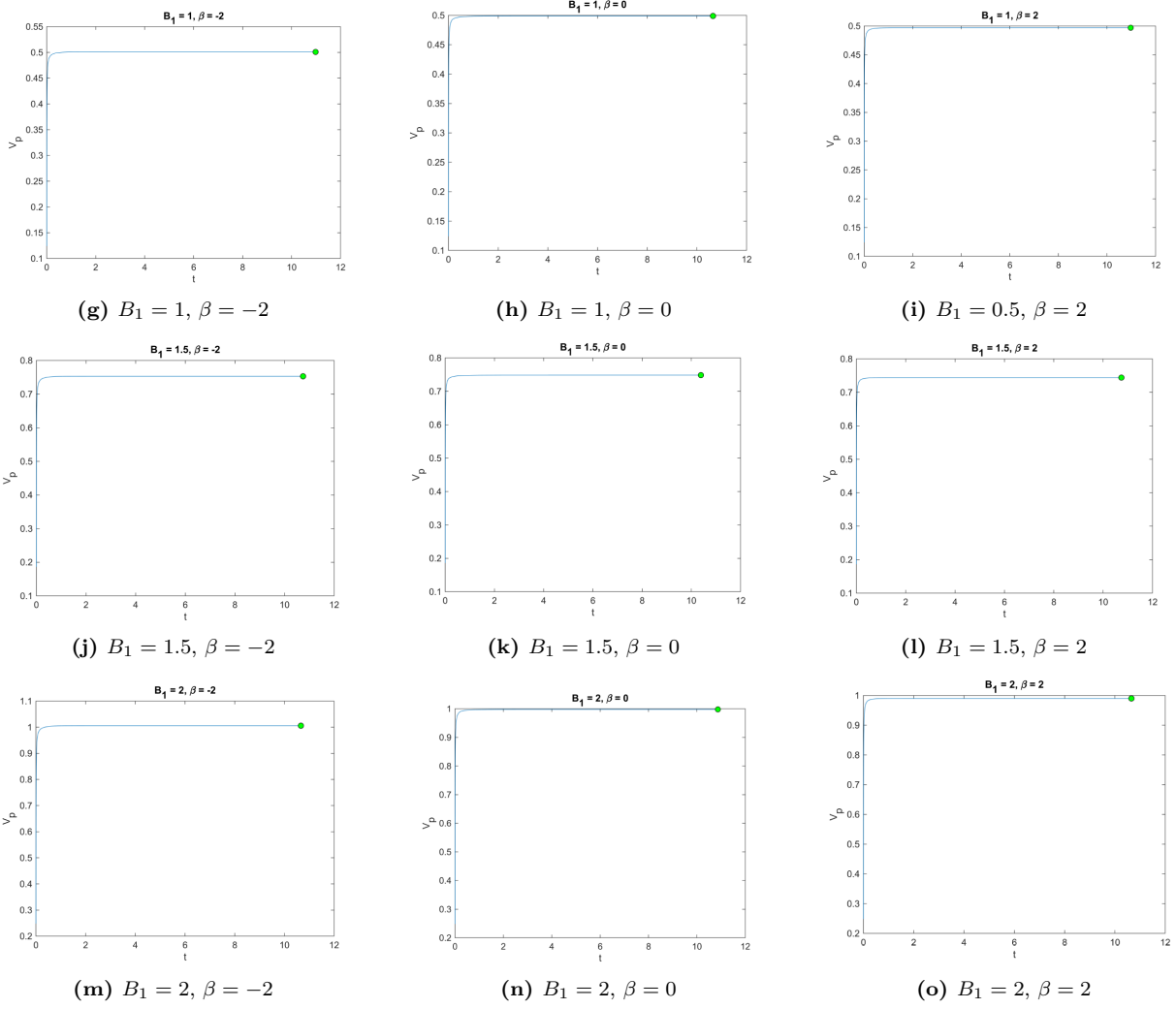


Figure 2.7: The non-dimensional velocity magnitude of the squirmer, \tilde{U}_s , as a function of non-dimensional time \tilde{t} for different values of B_1 and β . Each row corresponds to squirmers with a fixed value of B_1 , while each column represents a specific value of β characterizing the squirmer's self-propulsion mechanism as pusher ($\beta = -2$), neutral swimmer ($\beta = 0$), or puller ($\beta = 2$). The initial condition of $(\tilde{x}_0, \tilde{y}_0, \theta_0) = (25, 25, 0)$ is applied to the squirmer. The plots indicate that the velocity magnitude of the squirmer eventually attains a steady state value of $\frac{B_1}{2}$, in agreement with the theoretical value derived in Eqn. (2.5). Moreover, the plots suggest that the self-propulsion strength β has no significant effect on the velocity magnitude \tilde{U}_s as a function of time, for a given value of B_1 .

2.3.2 Variation of the x -component of squirmer's velocity with orientation angle θ

The x -component of the squirmer's non-dimensional velocity, \tilde{U}_x , is investigated in Fig. 2.8 as a function of orientational angle θ , for different values of B_1 and β . The plots are arranged in rows, representing squirmers with a fixed value of B_1 , while each column corresponds to a specific value of β that characterizes the squirmer's self-propulsion mechanism as pusher ($\beta = -2$), neutral swimmer ($\beta = 0$), or puller ($\beta = 2$). The results indicate that the x -component of the squirmer's velocity is invariant with respect to the orientational angle for any given values of B_1 and β , remaining constant at $\tilde{U}_x(\theta) = 1$ for all θ . This finding implies that the squirmer's motion is primarily in the direction of its symmetry axis, independent of its orientation in the fluid environment.

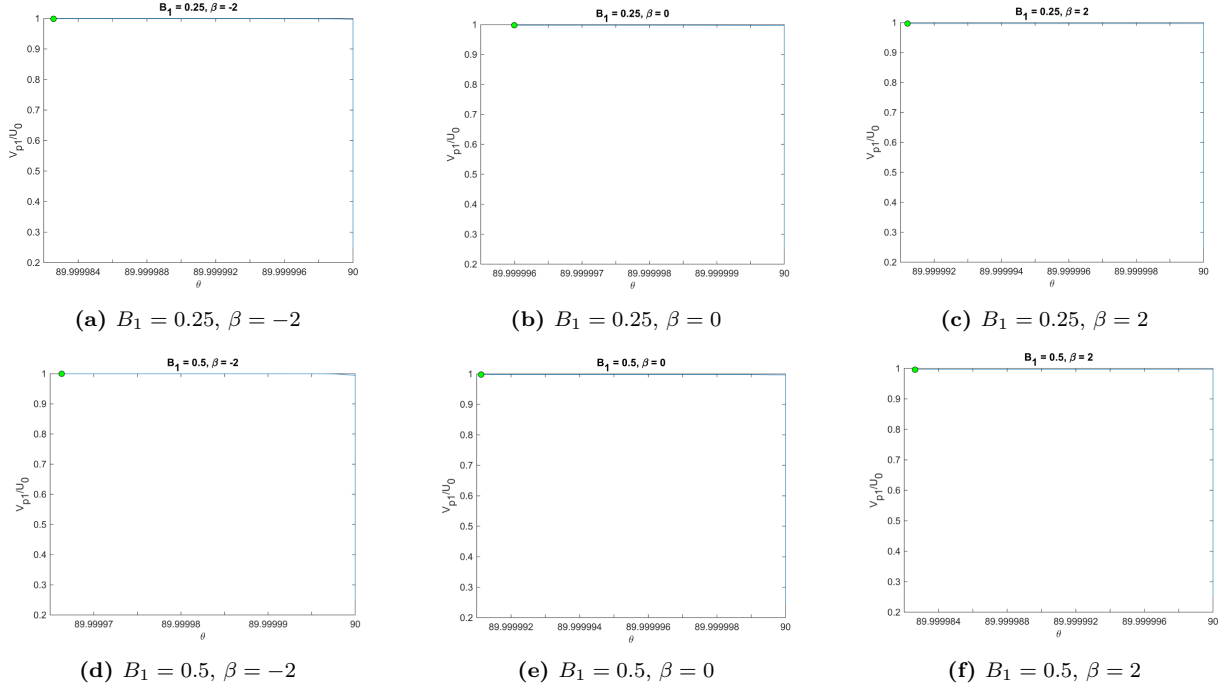


Figure 2.8

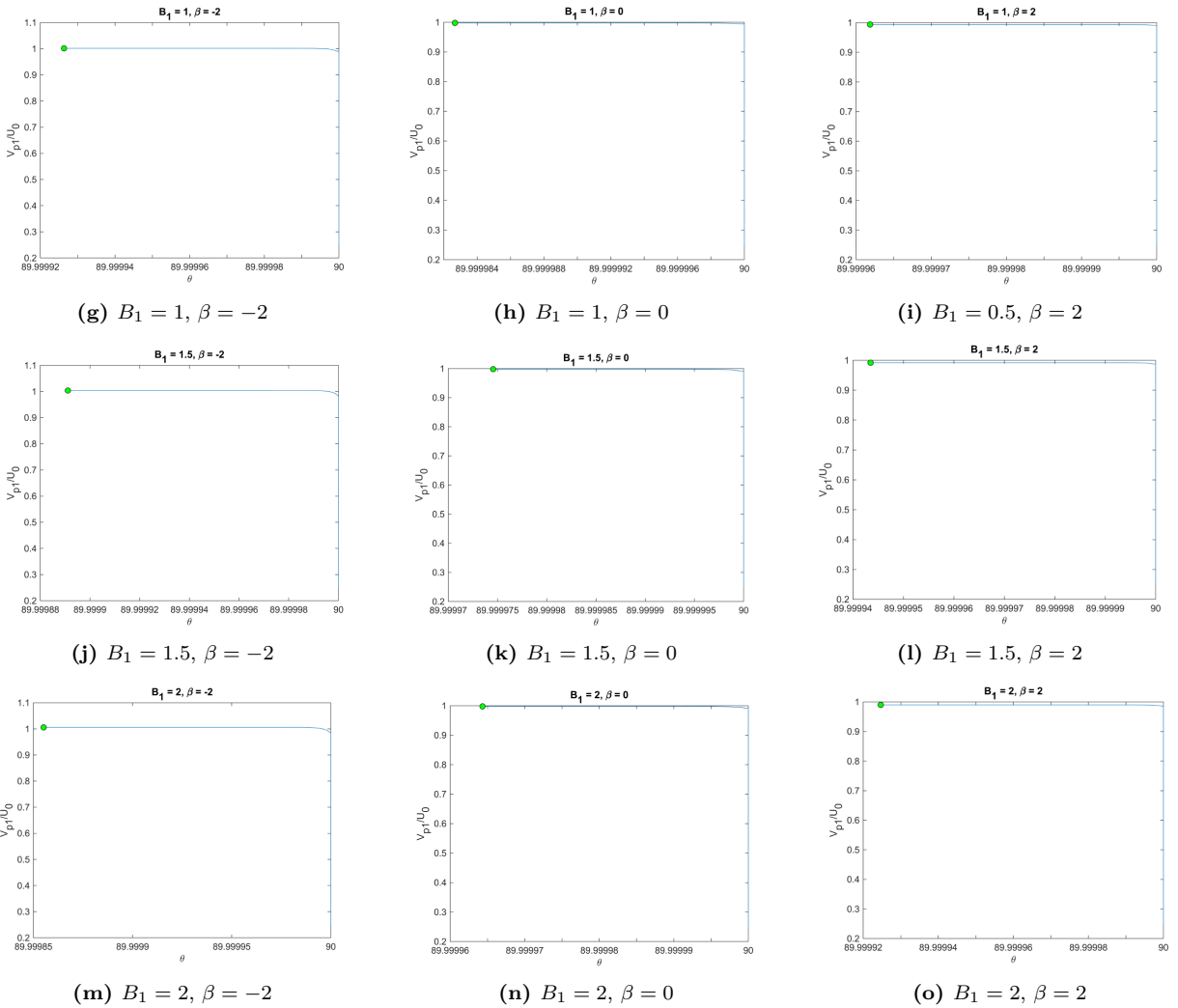


Figure 2.8: This figure displays the behavior of the non-dimensional x -component of the squirmer's velocity, \tilde{U}_x , as a function of the orientational angle θ , for various B_1 and β values. The plots are arranged in rows to represent squirmers with a fixed B_1 value, and each column corresponds to a specific β value characterizing the squirmer's self-propulsion as pusher ($\beta = -2$), neutral swimmer ($\beta = 0$), or puller ($\beta = 2$). The initial condition of $(\tilde{x}_0, \tilde{y}_0, \theta_0) = (25, 25, 0)$ is imposed on the squirmer. The results demonstrate that, irrespective of θ , \tilde{U}_x is constant at $\tilde{U}_x(\theta) = 1$ for all B_1 and β values, indicating that the squirmer predominantly moves along its symmetry axis, independent of its orientation in the fluid medium.

2.3.3 Variation of the y -component of squirmer's velocity with orientation angle θ

In this subsection, we investigate the y -component of the squirmer's non-dimensional velocity, \tilde{U}_y , as a function of orientational angle θ for different values of B_1 and β . The results are presented in Fig. 2.9, where each row corresponds to squirmers with a fixed value of B_1 , and each column represents a specific value of β characterizing the squirmer's self-propulsion mechanism as pusher ($\beta = -2$), neutral swimmer ($\beta = 0$), or puller ($\beta = 2$). Our findings reveal that as the first swimming mode B_1 increases, the rate of change of the squirmer's velocity in the y direction with respect to orientational angle also increases. Specifically, in pushers and neutral squirmers, \tilde{U}_y initially increases before showing a continuous decrease after reaching a maximum value. Conversely, in pullers, \tilde{U}_y initially decreases, but later increases continuously after reaching a minimum value. These results shed light on the intricate interplay between the squirmer's self-propulsion mechanism and the swimming gait in an infinite quiescent fluid, providing valuable insights for the design and control of micro- and nano-scale swimmers.

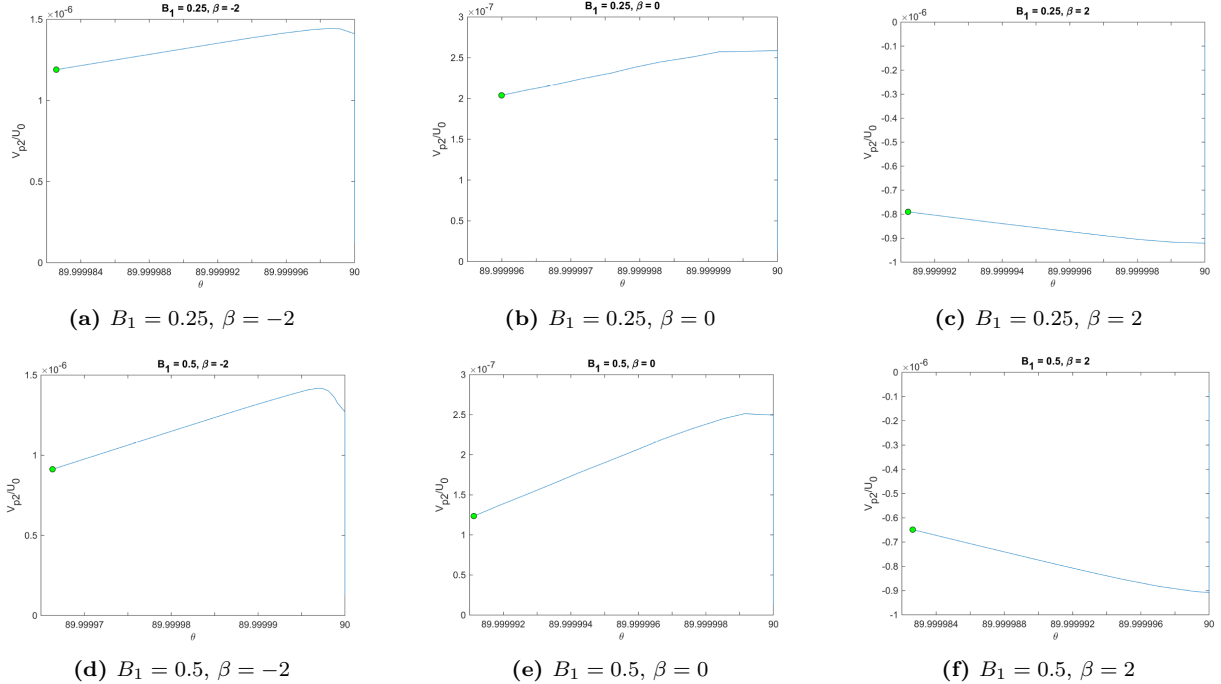


Figure 2.9

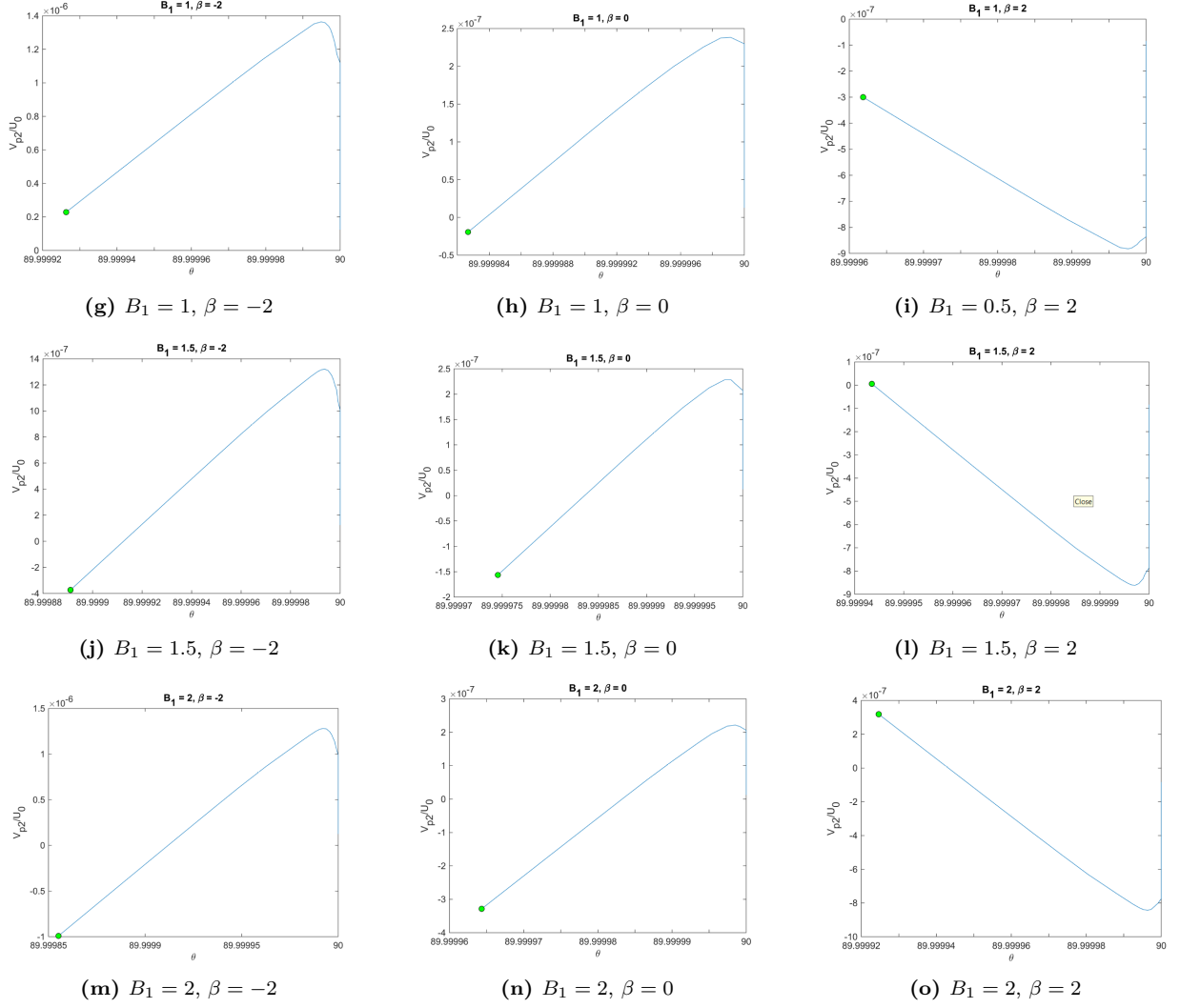


Figure 2.9: In this figure, the y -component of the squirmer's non-dimensional velocity, \tilde{U}_y , is plotted against orientational angle θ for different values of B_1 and β . Each row of the figure corresponds to squirmers with a fixed value of B_1 , and each column represents a specific value of β characterizing the squirmer's self-propulsion mechanism. The squirmer is initialized with $(\tilde{x}_0, \tilde{y}_0, \theta_0) = (25, 25, 0)$. Our results demonstrate that the rate of change of \tilde{U}_y with respect to orientational angle increases with the first swimming mode B_1 . Pushers and neutral squirmers exhibit an initial increase in \tilde{U}_y before showing a continuous decrease after reaching a maximum value. In contrast, pullers initially experience a decrease in \tilde{U}_y , which later increases continuously after reaching a minimum value.

2.3.4 Variation of the squirmer's rotational speed with orientation angle θ

In this subsection, we investigate the non-dimensional rotational speed, $\tilde{\Omega}$, of the squirmer as a function of the orientational angle, θ , for various values of B_1 and β . The results are presented in Fig. 2.10, where each row corresponds to squirmers with a constant value of B_1 , while each column represents a specific value of β , characterizing the squirmer as a pusher ($\beta = -2$), neutral swimmer ($\beta = 0$), or puller ($\beta = 2$). We observe that for a given value of B_1 and β , the non-dimensional rotational speed $\tilde{\Omega}$ is relatively constant with changes in the orientational angle θ , and the constant value depends only on the value of β . Specifically, for pushers with $\beta = -2$, $\tilde{\Omega}(\theta)$ attains a constant value, which is the same for all values of B_1 . Similar observations are made for neutral swimmers and pullers across all values of B_1 . Furthermore, the constant value is negative for pushers and neutral swimmers, indicating a clockwise constant rotational speed, while for pullers, the value is positive, indicating an anticlockwise constant rotational speed. We also note that with increasing B_1 , this constant value of $\tilde{\Omega}$ is attained at lower angles.

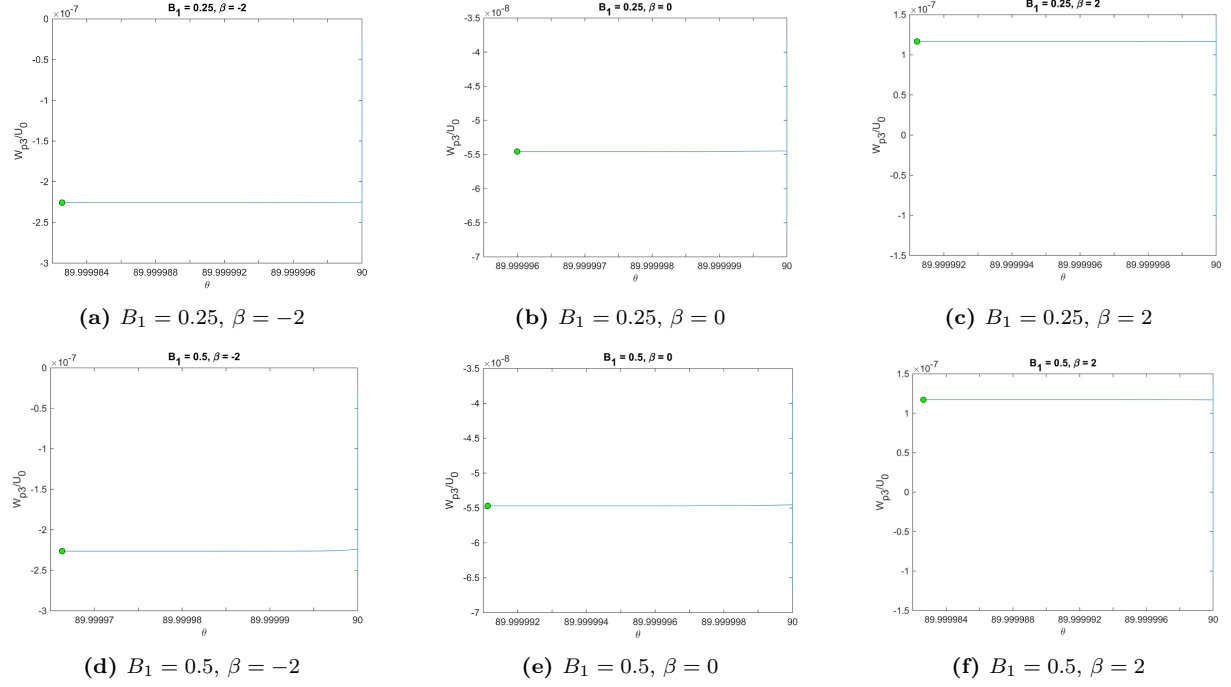


Figure 2.10

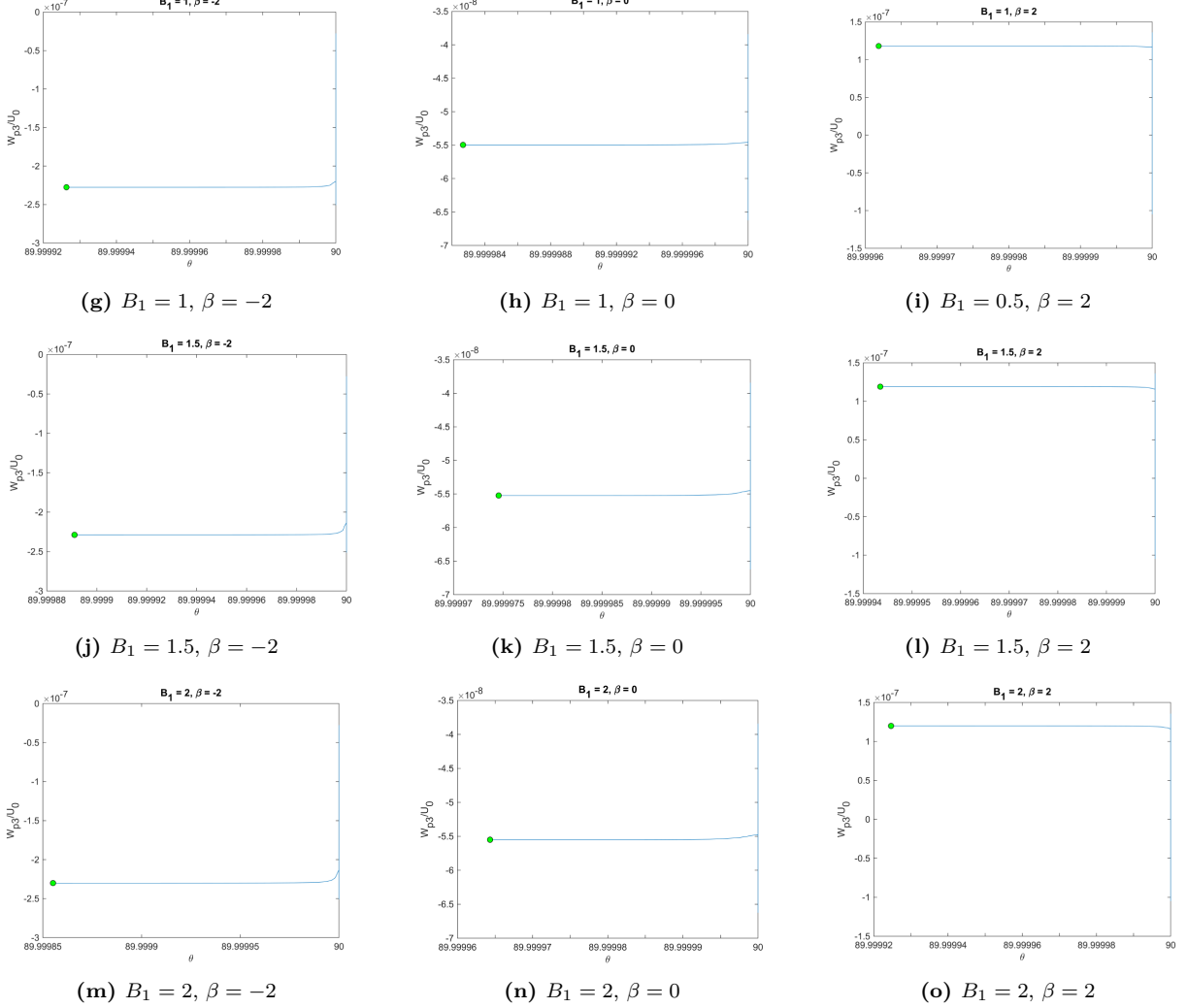


Figure 2.10: This figure displays the non-dimensional rotational speed, $\tilde{\Omega}$, of the squirmer as a function of the orientational angle, θ , for various values of B_1 and β . Each row in the figure corresponds to squirmers with a constant value of B_1 , while each column represents a specific value of β characterizing the squirmer's self-propulsion mechanism as a pusher ($\beta = -2$), neutral swimmer ($\beta = 0$), or puller ($\beta = 2$). The squirmer is initialized with $(\tilde{x}_0, \tilde{y}_0, \theta_0) = (25, 25, 0)$. The figure shows that for a given value of B_1 and β , the non-dimensional rotational speed $\tilde{\Omega}$ is relatively constant with changes in the orientational angle θ , and the constant value depends only on the value of β . Specifically, pushers and neutral swimmers have a negative constant value of $\tilde{\Omega}$, indicating a clockwise constant rotational speed, while pullers have a positive constant value, indicating an anticlockwise constant rotational speed. Moreover, with increasing B_1 , the constant value of $\tilde{\Omega}$ is attained at lower angles.

2.3.5 Velocity profile

Fig. 2.11 showcases the temporal evolution of the velocity field induced by a puller with a first swimming mode $B_1 = 2$ and self-propulsion strength $\beta = 2$ in an unbounded domain with quiescent fluid. The simulations were performed using COMSOL. The figure consists of three subfigures representing the velocity field at different time instances. The leftmost subfigure (Fig. 2.11a) corresponds to the initial time, the middle subfigure (Fig. 2.11b) represents an intermediate time, and the rightmost subfigure (Fig. 2.11c) displays the velocity field at the final time of the simulation. The magnitude of the flow velocity can be determined using the scale provided in Fig. 2.11d.

The streamlines depicted in the figures offer valuable insights into the propulsion mechanism of the puller at different time instances. Throughout the simulation, the puller consistently generates thrust in front of its body by extracting fluid from the front and back and ejecting it sideways.

Using our numerical simulation model, similar simulations can be conducted for other types of squirmers by considering different combinations of B_1 and β . In an unbounded quiescent fluid, pushers are observed to generate thrust behind their bodies by drawing fluid from the sides and propelling themselves through the liquid. On the other hand, neutral squirmers exhibit symmetric flow without any vorticity. These findings highlight the distinct propulsion mechanisms exhibited by different types of squirmers in an infinite fluid domain.

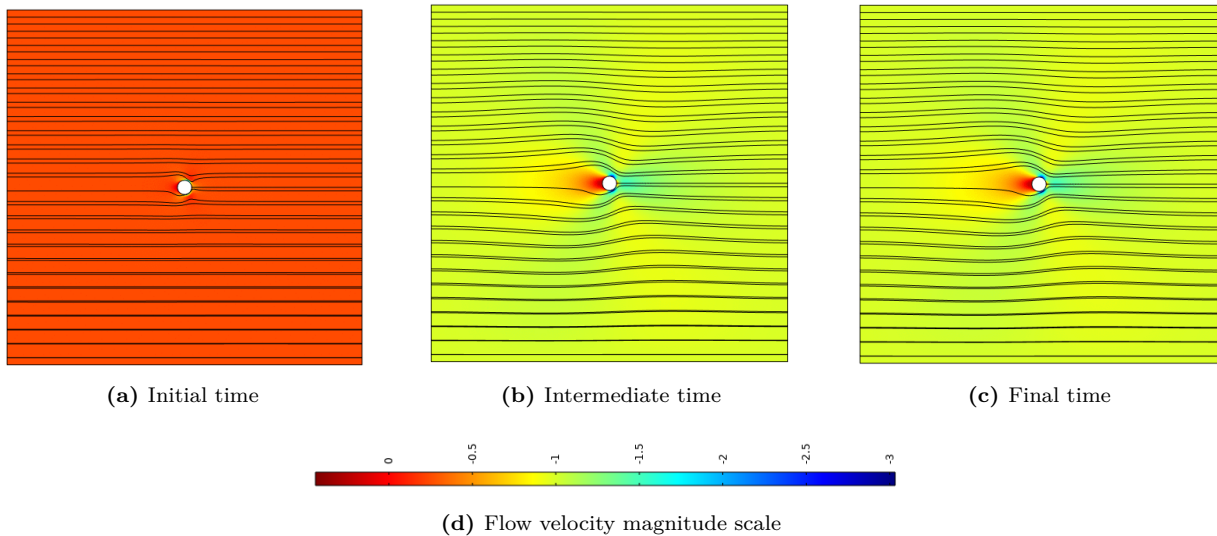


Figure 2.11: Temporal evolution of velocity fields induced by a puller with first swimming mode $B_1 = 2$ and self-propulsion strength $\beta = 2$ in an unbounded domain with quiescent fluid, as simulated using COMSOL. Black streamlines highlight propulsion mechanism at different time instances. Flow velocity magnitude scale is represented in (d).

Chapter 3

Swimming dynamics in a rectangular microchannel with quiescent fluid

3.1 Modelling a microswimmer in a rectangular microchannel with stationary fluid

3.1.1 Squirmer model

Similar to the methodology adopted in Chapter 2, we employed the squirmer model proposed by [11] and [12] to simulate the locomotion of a microswimmer in a quiescent fluid within a rectangular microchannel. The simplified squirmer model, characterized by a second-order truncated surface slip velocity, was also employed in this study and is expressed as:

$$\mathbf{u}^S(\mathbf{x}_s) = \sum_{n=0}^2 B_n \sin(n\theta) \hat{\mathbf{e}}_\theta = (B_1 \sin \theta + 2B_2 \sin \theta \cos \theta) \hat{\mathbf{e}}_\theta. \quad (3.1)$$

3.1.2 Domain specifications

A squirmer of radius a was considered, initially positioned at $\mathbf{x}_0 = (x_0, y_0)$ in a rectangular microchannel of length L and height H with a stationary fluid having density ρ and dynamic viscosity μ . The Reynolds number associated with the squirmer is given by

$$Re_s = \frac{\rho U_s a}{\mu} = \frac{\rho B_1 a}{2\mu}. \quad (3.2)$$

In order to replicate the aforementioned geometry in the laboratory frame, we positioned a two-dimensional rigid disk with radius a at $\mathbf{x}_0 = (x_0 = H, y_0 = 0)$ within a rectangular domain with a length of $L = 50a$ and height of $H = 10a$. This domain was filled with a fluid having density ρ , dynamic viscosity μ , and Reynolds number Re_s . The setup is shown in Fig. 3.1. The line $y = 0$ corresponds to the horizontal centreline of the domain. The top and bottom walls of the microchannel are represented by the lines $y = \pm H/2$ within the rectangular domain. The origin is located at the intersection of the horizontal centreline and the left boundary of the domain. The initial and boundary conditions of the fluid are prescribed as follows:

$$\text{IC 1: } \mathbf{u}(x, y, t) = \mathbf{0} \text{ at } 0 \leq x \leq L, -\frac{H}{2} \leq y \leq \frac{H}{2}, t = 0, \quad (3.3a)$$

$$\text{BC 1: } \mathbf{u}(x, y, t) = \mathbf{0} \text{ at } x = 0, -\frac{H}{2} \leq y \leq \frac{H}{2}, t \geq 0, \quad (3.3b)$$

$$\text{BC 2: } \mathbf{u}(x, y, t) = \mathbf{0} \text{ at } x = L, -\frac{H}{2} \leq y \leq \frac{H}{2}, t \geq 0, \quad (3.3c)$$

$$\text{BC 3 (no slip): } \mathbf{u}(x, y, t) = \mathbf{0} \text{ at } 0 \leq x \leq L, y = -\frac{H}{2}, t \geq 0, \quad (3.3d)$$

$$\text{BC 4 (no slip): } \mathbf{u}(x, y, t) = \mathbf{0} \text{ at } 0 \leq x \leq L, y = \frac{H}{2}, t \geq 0. \quad (3.3e)$$

(3.3)

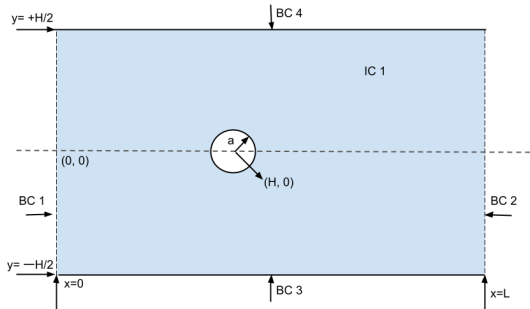


Figure 3.1: The figure depicts the initial configuration of a rectangular microchannel with a stationary fluid in the laboratory frame, containing a squirmers of radius a . The rectangular domain has a length of $L = 50a$ and a height of $H = 10a$, and is bounded by walls at $y = \pm H/2$. The squirmers, a two-dimensional disk with a radius of a , is positioned at $\mathbf{x}_0 = (H, 0)$ at the beginning of the simulation. The fluid velocity satisfies the initial and boundary conditions specified in Eqn. (3.3).

The fluid dynamics around the squirmer are governed by the incompressible Navier-Stokes equations, represented by Eqn. (2.9). The finite element method (FEM) is used once again to numerically solve these equations in software such as COMSOL or other appropriate simulation tools, as detailed in [19–21].

Simulating the motion of a squirmer in a small confined domain in the lab frame using simulation software such as COMSOL can be challenging. However, a relatively simple solution involves observing the motion from a different reference frame, called the *x-moving frame*. This reference frame translates only in the *x* direction with a speed U_x , which is the *x* component of the squirmer's velocity. It is important to note that the *x*-moving frame is devoid of any rotational velocity.

To mimic the motion of a squirmer in a rectangular microchannel filled with a stagnant fluid, we placed a non-deformable two-dimensional disk with a radius of a at $\mathbf{x}_0 = (x_0 = H, y_0 = 0)$ within a rectangular domain with a length of either $L = 16a$ or $L = 20a$, and a height of $H = L/2$. The fluid within the domain has a density of ρ , dynamic viscosity of μ , and Reynolds number of Re_s . The configuration is illustrated in Fig. 3.2, where the horizontal centreline of the domain is represented by the line $y = 0$. In this frame, the top and bottom walls of the microchannel are seen to move with a velocity $-U_x \hat{\mathbf{e}}_x$ and are denoted by the lines $y = \pm H/2$ within the rectangular domain. The origin is located at the intersection of the horizontal centreline and the left boundary of the domain. To reflect the changes made in the frame, we adapted the initial and boundary conditions of the fluid as described below:

$$\text{IC 1: } \mathbf{u}(x, y, t) = -U_{x0} \hat{\mathbf{e}}_x \text{ at } 0 \leq x \leq L, \quad -\frac{H}{2} \leq y \leq \frac{H}{2}, \quad t = 0, \quad (3.4a)$$

$$\text{BC 1: } \mathbf{u}(x, y, t) = -U_{x,t} \hat{\mathbf{e}}_x \text{ at } x = 0, \quad -\frac{H}{2} \leq y \leq \frac{H}{2}, \quad t \geq 0, \quad (3.4b)$$

$$\text{BC 2: } \mathbf{u}(x, y, t) = -U_{x,t} \hat{\mathbf{e}}_x \text{ at } x = L, \quad -\frac{H}{2} \leq y \leq \frac{H}{2}, \quad t \geq 0, \quad (3.4c)$$

$$\text{BC 3: } \mathbf{u}(x, y, t) = -U_{x,t} \hat{\mathbf{e}}_x \text{ at } 0 \leq x \leq L, \quad y = -\frac{H}{2}, \quad t \geq 0, \quad (3.4d)$$

$$\text{BC 4: } \mathbf{u}(x, y, t) = -U_{x,t} \hat{\mathbf{e}}_x \text{ at } 0 \leq x \leq L, \quad y = \frac{H}{2}, \quad t \geq 0, \quad (3.4e)$$

(3.4)

where U_{x0} denotes the *x*-component of the squirmer velocity at the initial time $t = 0$, while $U_{x,t}$ denotes the *x*-component of the squirmer velocity at any subsequent time t .

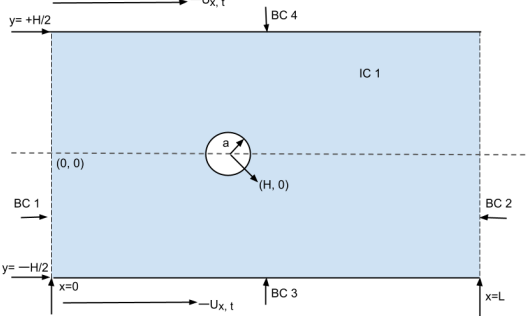


Figure 3.2: The figure illustrates the initial configuration of a rectangular microchannel in the x -moving frame, containing a stationary fluid and a squirmer of radius a . The rectangular domain has a length of either $L = 16a$ or $L = 20a$ and a height of $H = L/2$. The walls located at $y = \pm H/2$ move with a velocity $-U_x \hat{e}_x$. At the start of the simulation, the squirmer, a non-deformable two-dimensional disk with radius a , is positioned at $\mathbf{x}_0 = (H, 0)$. The initial and boundary conditions for the fluid velocity are described in Eqn. (3.4).

It should be noted that despite the change of frame (from the lab frame to the x -moving frame), the fluid dynamics around the squirmer remains unchanged. Therefore, the equations governing the fluid dynamics are still described by the incompressible Navier-Stokes equations as previously described in Eqn. (2.9).

3.2 Numerical method

3.2.1 Squirmer dynamics

The position of the squirmer at a specific time is represented by a position vector $\mathbf{x} = x\hat{e}_x + y\hat{e}_y$, and its instantaneous orientation is indicated by the unit vector $\hat{\mathbf{e}} = e_x\hat{e}_x + e_y\hat{e}_y$, as shown in Fig. 3.3. The translational velocity of the squirmer is given by $\mathbf{U}_s = U_x\hat{e}_x + U_y\hat{e}_y$, and its rotational velocity is given by $\boldsymbol{\Omega} = \Omega\hat{e}_z$.

The surface velocity \mathbf{u}_s at any point \mathbf{x}_s on the squirmer surface in the lab frame is expressed in Eqn. (2.11). The governing equations of motion (EOMs) and component-wise EOMs for the squirmer motion in the microchannel in the lab frame are identical to those described by Eqns. (2.12) and (2.14).

In order to investigate the squirmer's motion in the x -moving frame, it is crucial to express the squirmer surface velocity and governing EOMs appropriately. In this frame, the surface

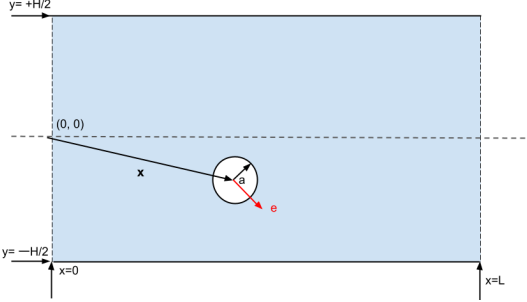


Figure 3.3

velocity of the squirmer is expressed as follows:

$$\begin{aligned}\mathbf{u}_s(\mathbf{x}_s) &= \mathbf{u}^S(\mathbf{x}_s) + U_y \hat{\mathbf{e}}_y + \boldsymbol{\Omega} \times \mathbf{x}_s \\ &= B_1 (\sin \theta + 2\beta \sin \theta \cos \theta) \hat{\mathbf{e}}_\theta + U_y \hat{\mathbf{e}}_y + \boldsymbol{\Omega} \times \mathbf{x}_s.\end{aligned}\quad (3.5)$$

The component-wise EOMs in the x -moving frame can be obtained by applying an appropriate transformation to the EOMs in the lab frame, as described below:

$$\frac{dy}{dt} = U_y, \quad (3.6a)$$

$$\frac{de_x}{dt} = -\Omega e_y, \quad \frac{de_y}{dt} = \Omega e_x, \quad (3.6b)$$

$$\frac{dU_y}{dt} = \frac{1}{m} \iint_A f_y(\mathbf{x}_s) dA, \quad (3.6c)$$

$$\frac{d\Omega}{dt} = \frac{1}{J} \iint_A [x_{sx} f_y - x_{sy} f_x] dA, \quad (3.6d)$$

(3.6)

In this frame, the x -component of the squirmer's velocity is constantly zero. As a result, only the EOMs governing the y -component of the translational velocity and acceleration, as well as the rotational velocity and acceleration, are pertinent, as indicated in Eqn. (3.6).

3.2.2 Non-dimensionalisation

In order to establish a dimensionless representation of the system, suitable scaling factors are introduced to relevant physical quantities. Specifically, all length variables are scaled by the radius of the squirmer a , all velocity variables are scaled by the steady-state swimming speed of the squirmer in an infinite quiescent fluid medium $U_s = B_1/2$, the time variable is scaled by a/U_s , and all force variables are scaled by mU_s^2/a . Consequently, the same non-dimensional variables as given in Eqn. (2.18) are defined. Additionally, the following non-dimensional constants are introduced:

$$\tilde{x}_0 = x_0/a, \quad \tilde{y}_0 = y_0/a, \quad \tilde{L} = L/a, \quad \tilde{H} = H/a. \quad (3.7)$$

By adopting the above non-dimensionalisation, the same non-dimensional lab frame component-wise EOMs described by Eqn. (2.20) are obtained. Similarly, the non-dimensionalized component-wise EOMs in the x -moving frame can be derived from the x -moving frame EOMs given in Eqn. (3.6) after applying the same non-dimensionalization, and are expressed as follows:

$$\frac{d\tilde{y}}{d\tilde{t}} = \tilde{U}_y, \quad (3.8a)$$

$$\frac{de_x}{d\tilde{t}} = -\tilde{\Omega}e_y, \quad \frac{de_y}{d\tilde{t}} = \tilde{\Omega}e_x, \quad (3.8b)$$

$$\frac{d\tilde{U}_y}{d\tilde{t}} = \iint_A \tilde{f}_y(\mathbf{x}_s/a) dA, \quad (3.8c)$$

$$\frac{d\tilde{\Omega}}{d\tilde{t}} = 2 \iint_A [\tilde{x}_{sx}\tilde{f}_y - \tilde{x}_{sy}\tilde{f}_x] dA. \quad (3.8d)$$

(3.8)

3.2.3 Wall-induced hydrodynamic interactions

Past studies have compared the behavior of swimmers in unconfined and confined environments and have demonstrated that the presence of a wall can have a significant impact on the velocity of the model squirmer in both the parallel (U_x) and perpendicular (U_y) directions [3, 9, 22]. This variation in velocity can be attributed to wall-induced attraction or repulsion of the squirmer due to hydrodynamic interactions. The direction of the induced velocity depends on the orientation of the squirmer near the wall. Furthermore, observations have revealed that a squirmer near a wall undergoes rotation, with the direction of

rotation causing the squirmer to orient itself away from the wall. Consequently, hydrodynamic interactions between a squirmer and a wall can result in attraction or repulsion and reorientation, ultimately leading to a hydrodynamic collision with the wall.

The hydrodynamic interactions between a two-dimensional squirmer and a no-slip wall have been fully characterized in [22]. These interactions are described by the exact expressions presented as follows:

$$\frac{d\tilde{x}}{d\tilde{t}} = \frac{1}{2}(1 - \lambda^2) [-B_1 \sin \theta + 2\lambda B_2 \sin(2\theta)], \quad (3.9a)$$

$$\frac{d\tilde{y}}{d\tilde{t}} = \frac{(1 - \lambda^2)^2}{2(1 + \lambda^2)} [B_1 \cos \theta + 2\lambda B_2 \sin(2\theta)], \quad (3.9b)$$

$$\frac{d\hat{\mathbf{e}}_x}{d\tilde{t}} = \frac{\lambda^2}{1 + \lambda^2} [2\lambda B_1 \sin \theta - (1 - 3\lambda^2) B_2 \cos(2\theta)] \sin \theta, \quad (3.9c)$$

$$\frac{d\hat{\mathbf{e}}_y}{d\tilde{t}} = \frac{\lambda^2}{1 + \lambda^2} [-2\lambda B_1 \sin \theta + (1 - 3\lambda^2) B_2 \cos(2\theta)] \cos \theta, \quad (3.9d)$$

where $\lambda = \tilde{h} - (\tilde{h}^2 - 1)^{1/2}$, and $\tilde{h} = \frac{\tilde{H}}{2} - |\tilde{y}|$ represents the non-dimensional distance of the squirmer's center from the nearer wall.

3.2.4 Wall induced non-hydrodynamic interactions

To prevent collisions between a body and a wall, hydrodynamic interactions alone are not always sufficient. To address this, we introduce a screened electrostatic-type (non-hydrodynamic) repulsion force that operates only at small distances from the boundary, as discussed in previous studies such as [3, 23, 24]. This force is given by

$$\mathbf{F}_{rep} = -F_{rep}\hat{\mathbf{e}}_y = -\frac{Ae^{-Bd}}{1 - e^{-Bd}}\hat{\mathbf{e}}_y, \quad (3.10)$$

where $d = \left| \frac{\tilde{H}}{2} - \tilde{x}_y - 1 \right|$ is the minimum non-dimensional distance between the body surface of the squirmer and the nearest wall.

Fig. 3.4 shows the increasing magnitude of the force F_{rep} as the minimum distance d decreases, for different values of the parameters A and B . The chosen values of A and B in Fig. 3.4 ensure that the squirmer cannot approach closer to the wall than $d = 0.25$, beyond which the accuracy of numerical methods for computing fluid velocity in simulation

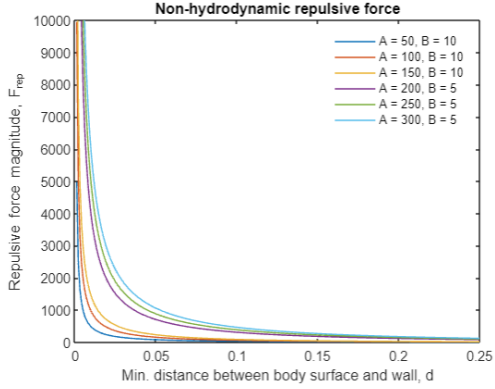


Figure 3.4: Plot showing the variation of the magnitude of the non-hydrodynamic repulsive force, denoted by F_{rep} , as a function of the minimum distance d between the surface of the squirmer's body and the nearest wall, for different combinations of the parameters A and B .

software such as COMSOL begins to decrease (albeit slightly, as discussed in [25]). More physically realistic near-contact interaction effects are discussed by [26].

To incorporate the non-hydrodynamic repulsive force, described by Eqn. (3.4), into the non-dimensionalized EOMs of the lab frame and the x -moving frame, the existing equations, given by Eqns. (2.20) and (3.8), respectively, can be used with a modification in the y -component of the translational acceleration. Specifically, the y -component of the acceleration can be rewritten in non-dimensional form as shown below:

$$\frac{d\tilde{U}_y}{d\tilde{t}} = \iint_A \tilde{f}_y(\mathbf{x}_s/a) dA - F_{rep}. \quad (3.11)$$

As described in Chapter 2, the non-dimensionalized component-wise governing EOMs can be solved numerically using the Euler's method with suitable initial conditions.

3.2.5 Simulation parameters for the x -moving frame

This section provides an overview of the simulation parameters used for the x -moving frame. The simulations are conducted on a domain size of either 8×16 or 10×20 , unless otherwise specified. The boundary conditions described in Eqn. (3.4) are imposed on the bottom and top walls, as well as the remaining two sides of the domain. To solve the Navier-Stokes equations in Eqn. (2.9) using the finite element method (FEM), spatial and temporal resolutions are set to unity, following standard FEM practices. The density and dynamic viscosity of the Newtonian fluid are assigned values of $\rho = Re_s = 0.01$ and $\mu = 1$, respectively, all in lattice units.

A single squirmer with a radius of 1 lattice unit is initially placed at $(\tilde{x}_0, \tilde{y}_0) = (8, 0)$ with an initial orientation θ_0 . An iterative procedure, such as Euler's method, is employed to calculate the squirmer's position and components of squirmer velocity using the non-dimensional governing equations of motion (EOMs) in Eqns. (2.20) and (3.8) based on the steady-state flow fields obtained using FEM. The iterative procedure continues until a puller of the first swimming mode $B_1 = 2$ and self-propulsion strength $\beta = 1$ reaches a steady-state value of the velocity magnitude at time t_F , or until a non-dimensional time of 1000 is reached. The time step used for this iterative procedure is set to $\Delta t = 1$.

For the FEM, the mesh elements are defined as free triangular, with a maximum size of 0.02 near the squirmer's surface, as well as the top and bottom walls. In the rest of the domain, the maximum mesh size is set to 1, as illustrated in Fig. 3.5. Additionally, to account for the vertical motion of the squirmer, the deformed mesh feature in COMSOL is enabled. Moreover, to ensure accurate simulation results, automatic remeshing is enabled.

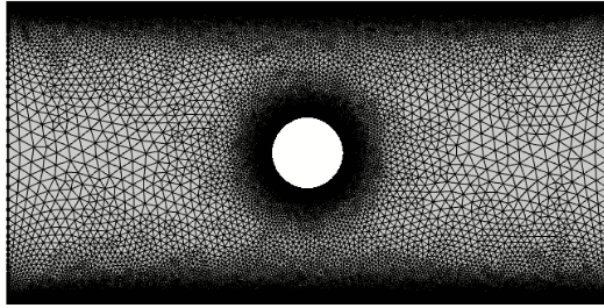


Figure 3.5: Mesh used in the simulations in the co-moving frame, with maximum element size of 1 for the majority of the domain and 0.02 near the squirmer's surface and top/bottom walls. The mesh is shown for a simulation domain of 8×16 .

3.3 Results and discussion

3.3.1 Confinement induced trajectories

The trajectories of squirmers with a first swimming mode $B_1 = 2$ and various self-propulsion strengths β ($\beta = -2, -1, \dots, 2$) in a rectangular microchannel with quiescent fluid are shown in Fig. 3.6. All trajectories in Fig. 3.6 begin at the initial condition $(\tilde{x}, \tilde{y}, \theta) = (H, 0, \pi/4)$.

It can be observed from Fig. 3.6 that squirmers with $\beta = -2$ and $\beta = -1$ (pushers with $\beta < 0$) exhibit an oscillatory behavior with minimal decay in amplitude. Additionally, the frequency of oscillations in the trajectory of the squirmer with $\beta = -1$ is greater than that of the squirmer with $\beta = -2$, indicating an increase in oscillatory behavior for pushers as β increases.

Neutral squirmers with $\beta = 0$ display an oscillatory trajectory similar to pushers, but with a small and non-negligible decay in amplitude.

Finally, puller squirmers with $\beta = 1$ and $\beta = 2$ exhibit oscillatory behavior with high decay in amplitude, ultimately leading to a straight trajectory along the centre of the rectangular channel. The rate of decay of the amplitude increases with an increase in β for pullers.

The above findings are consistent with previous research studies such as [9, 27, 28], which support the accuracy of our numerical simulation model. Thus, we can conclude that our model is reliable and can be used for further studies.

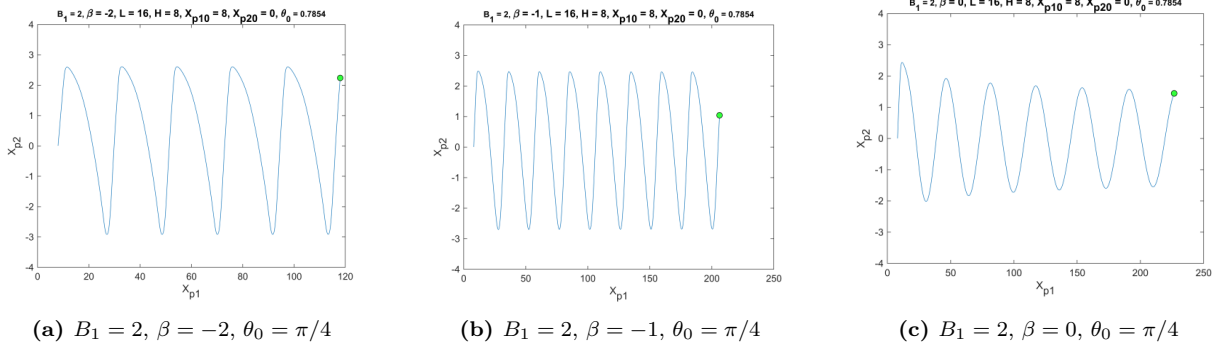


Figure 3.6

3.3.2 Time evolution of the squirmer's velocity magnitude

Fig. 3.7 depicts the magnitude of velocity (U_p) of squirmers in a rectangular microchannel with quiescent fluid, as a function of time, for various self-propulsion strengths (β). The plots in the figure correspond to squirmers with a first swimming mode $B_1 = 2$ and start from an initial condition of $(\tilde{x}, \tilde{y}, \theta) = (H, 0, \pi/4)$.

The results in Fig. 3.7 indicate that pusher squirmers ($\beta < 0$) with $\beta = -2$ and $\beta = -1$ exhibit oscillatory behavior in the magnitude of velocity with time. These squirmers display negligible decay in the amplitude of the oscillations, indicating that U_p never reaches a

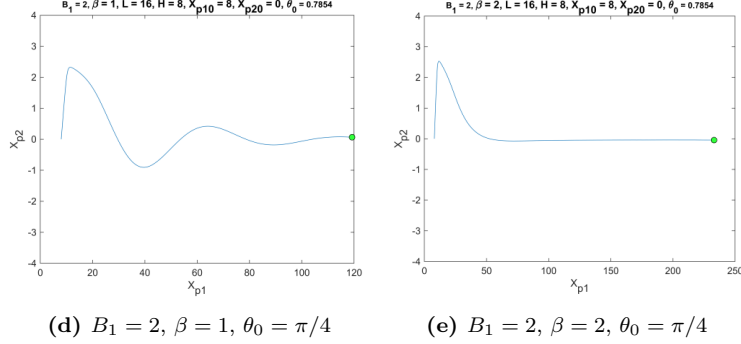


Figure 3.6: Trajectories of squirmers with $B_1 = 2$ and varying β values in a rectangular microchannel with quiescent fluid. Squirmers with negative β values are pushers while those with positive β values are pullers. The initial condition for all trajectories is $(\tilde{x}, \tilde{y}, \theta) = (H, 0, \pi/4)$.

steady-state value. Furthermore, the frequency of oscillations in the velocity magnitude-time plot of the squirmer with $\beta = -1$ is higher than that of the squirmer with $\beta = -2$, suggesting an increase in oscillatory behavior with increasing β for pushers.

Neutral squirmers with $\beta = 0$ also show oscillatory behavior in the magnitude of velocity, similar to pushers. However, the amplitude of oscillations decays slowly with time, indicating that U_p would reach a steady-state value in infinite time.

In contrast, puller squirmers ($\beta > 0$) with $\beta = 1$ and $\beta = 2$ exhibit oscillatory behavior with high decay in amplitude. The magnitude of velocity ultimately reaches a steady-state value, which differs from the steady-state value of $U_s = B_1/2$ for squirmers in an infinite quiescent fluid. This behavior suggests that confinement or hydrodynamic and non-hydrodynamic interactions of the squirmer with the channel walls play a significant role in the motion of the squirmer. The rate of decay of amplitude increases with an increase in β for pullers, as observed from the plots in Fig. 3.7.

3.3.3 Variation of the x and y -component of squirmer's velocity with orientation angle θ

Figs. 3.8 and 3.9 illustrate the squirmer's velocity components, namely the x -component U_x and y -component U_y , respectively, in a rectangular microchannel filled with quiescent fluid, as a function of the orientation angle θ for varying self-propulsion strengths (β). In both figures, the squirmers belong to the first swimming mode $B_1 = 2$ and start from the initial condition of $(\tilde{x}, \tilde{y}, \theta) = (H, 0, \pi/4)$.

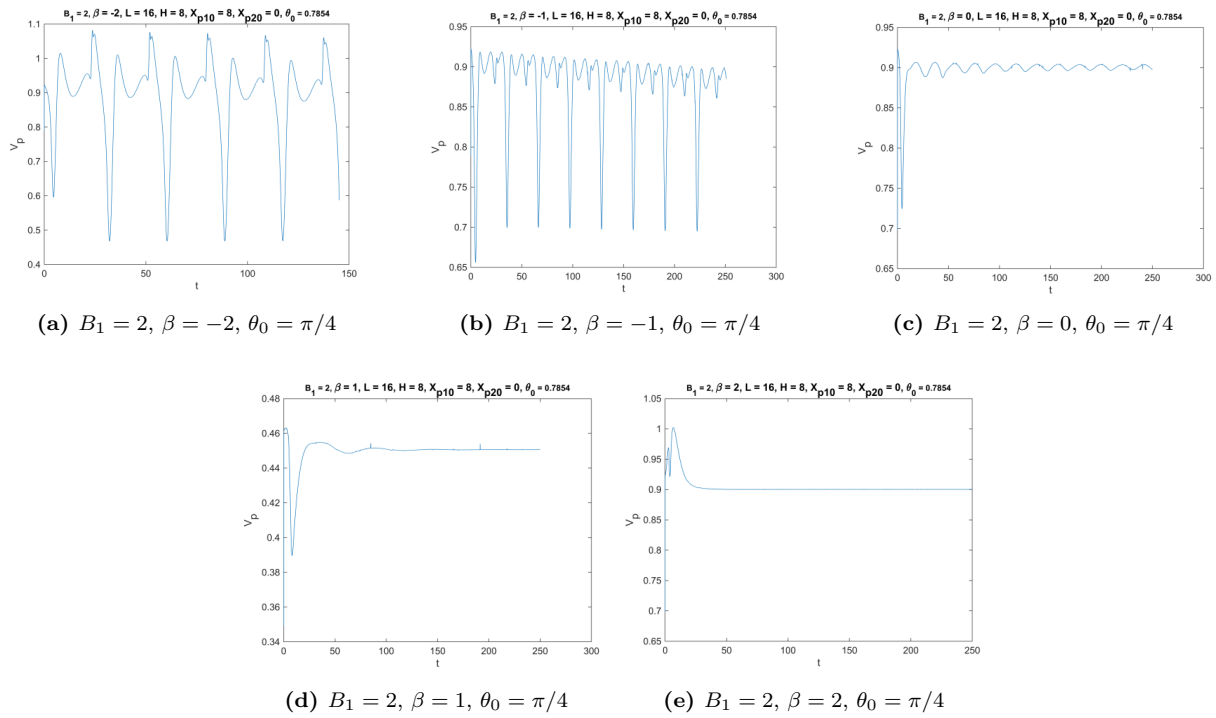


Figure 3.7: The figure illustrates the temporal evolution of the magnitude of velocity U_p for squirmers with first swimming mode $B_1 = 2$ and varying self-propulsion strengths β in a rectangular microchannel with quiescent fluid. The plots are initialized with $(\tilde{x}, \tilde{y}, \theta) = (H, 0, \pi/4)$ for all cases. The figure shows that squirmers with different values of β exhibit distinct oscillatory behaviors with time, and the rate of decay in the amplitude of the oscillations depends on the type of squirmer and the value of β .

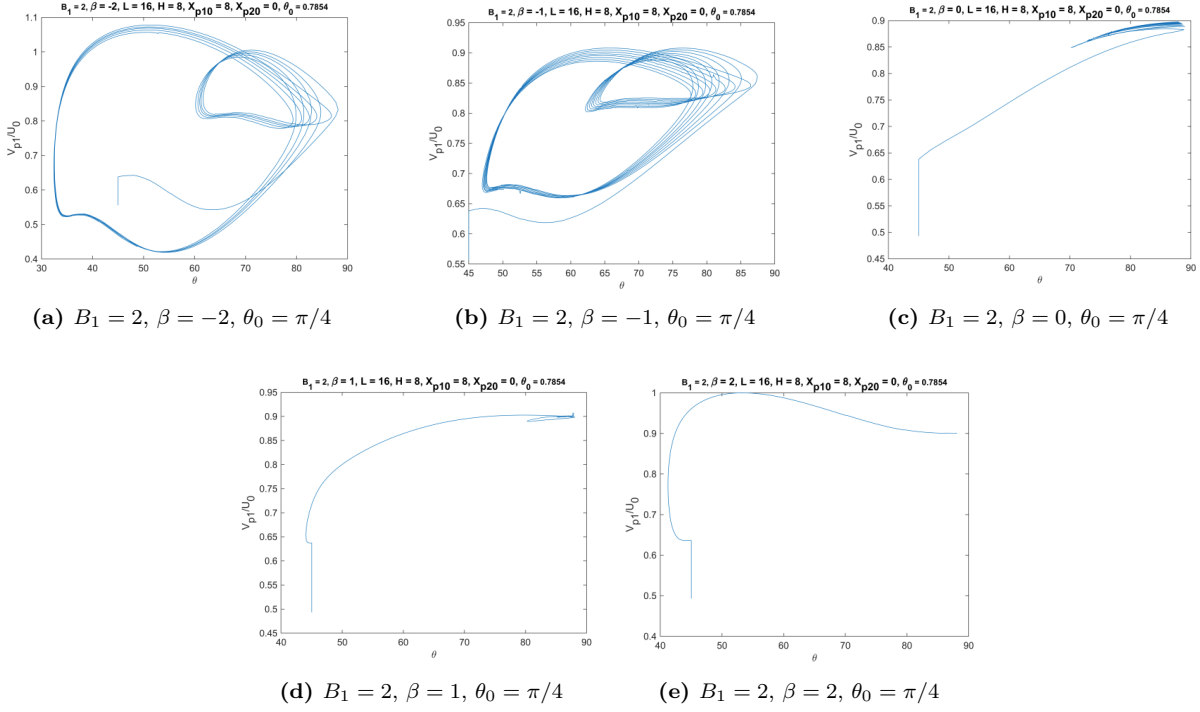


Figure 3.8: x -component of the velocity, U_x , of squirmers with first swimming mode $B_1 = 2$ and different self-propulsion strengths β as a function of orientation angle θ in a rectangular microchannel with quiescent fluid. The initial condition for all plots is $(\tilde{x}, \tilde{y}, \theta) = (H, 0, \pi/4)$.

Upon observing the plots of pushers ($\beta = -2, -1$) in Figs. 3.8 and 3.9, it is evident that these squirmers display an oscillatory trajectory and velocity magnitude that decays over time. This behavior aligns with the expected dynamics of pusher squirmers, as their self-propulsion forces generate periodic motion with decaying oscillations. Similarly, the neutral squirmer ($\beta = 0$) also demonstrates an oscillatory trajectory and velocity magnitude, with a small but noticeable decay in the amplitude of oscillations. These findings highlight that even in the absence of a net propulsive force, neutral squirmers still exhibit periodic motion with an amplitude that gradually diminishes.

In contrast, the plots of pullers ($\beta = 1, 2$) in both figures exhibit a different behaviour. Here, the amplitude of oscillations in the velocity component decreases rapidly over time until it reaches a steady-state value. This observation implies that the puller squirmers achieve a stable motion pattern with a fixed amplitude of oscillations, unlike the oscillatory behavior seen in pushers and neutral squirmers.

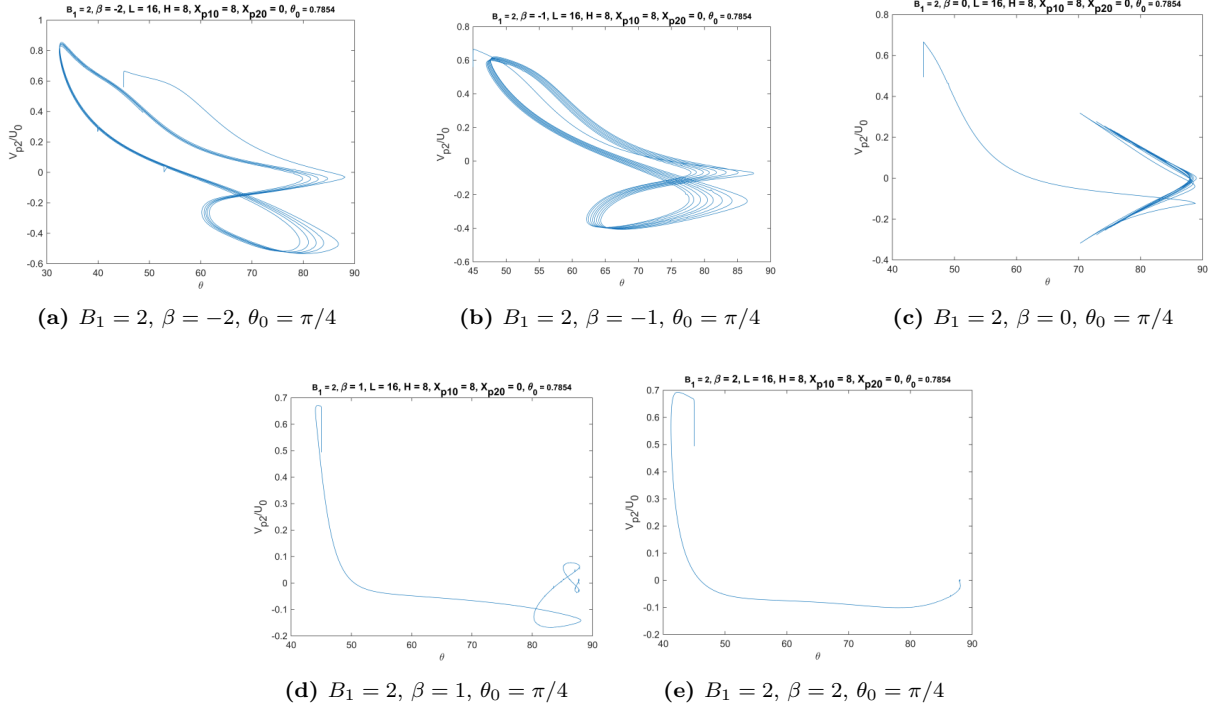


Figure 3.9: y -component of the velocity, U_y , of squirmers with first swimming mode $B_1 = 2$ and different self-propulsion strengths β as a function of orientation angle θ in a rectangular microchannel with quiescent fluid. The initial condition for all plots is $(\tilde{x}, \tilde{y}, \theta) = (H, 0, \pi/4)$.

3.3.4 Velocity profile

Fig. 3.10 presents the temporal evolution of the velocity field induced by a squirmer with a first swimming mode $B_1 = 2$ in a rectangular microchannel containing quiescent fluid. The figure displays velocity fields for different self-propulsion strengths (β), categorized into three columns: pusher ($\beta = -2$), neutral squirmer ($\beta = 0$), and puller ($\beta = 2$). Each row represents the velocity field at different time instances: the top row corresponds to the beginning of the simulation, the middle row represents an intermediate time, and the bottom row shows the velocity field at the end of the simulation. The flow velocity magnitude scale can be referred to in Fig. 3.10j.

In this visualization, the black lines depict streamlines that provide valuable insights into the propulsion mechanisms exhibited by each type of squirmer at different time points. It is evident that the pusher generates thrust behind its body by drawing fluid from the sides and propelling itself through the liquid. On the contrary, the puller generates thrust in

front of its body by extracting fluid from the front and back and ejecting it sideways. The neutral squirmer, in contrast, demonstrates symmetric flow without any vorticity. Notably, the velocity fields of all types of squirmers exhibit notable variations over time, reflecting the influence of the self-propulsion strength and the hydrodynamic and non-hydrodynamic interactions with the channel's top and bottom walls.

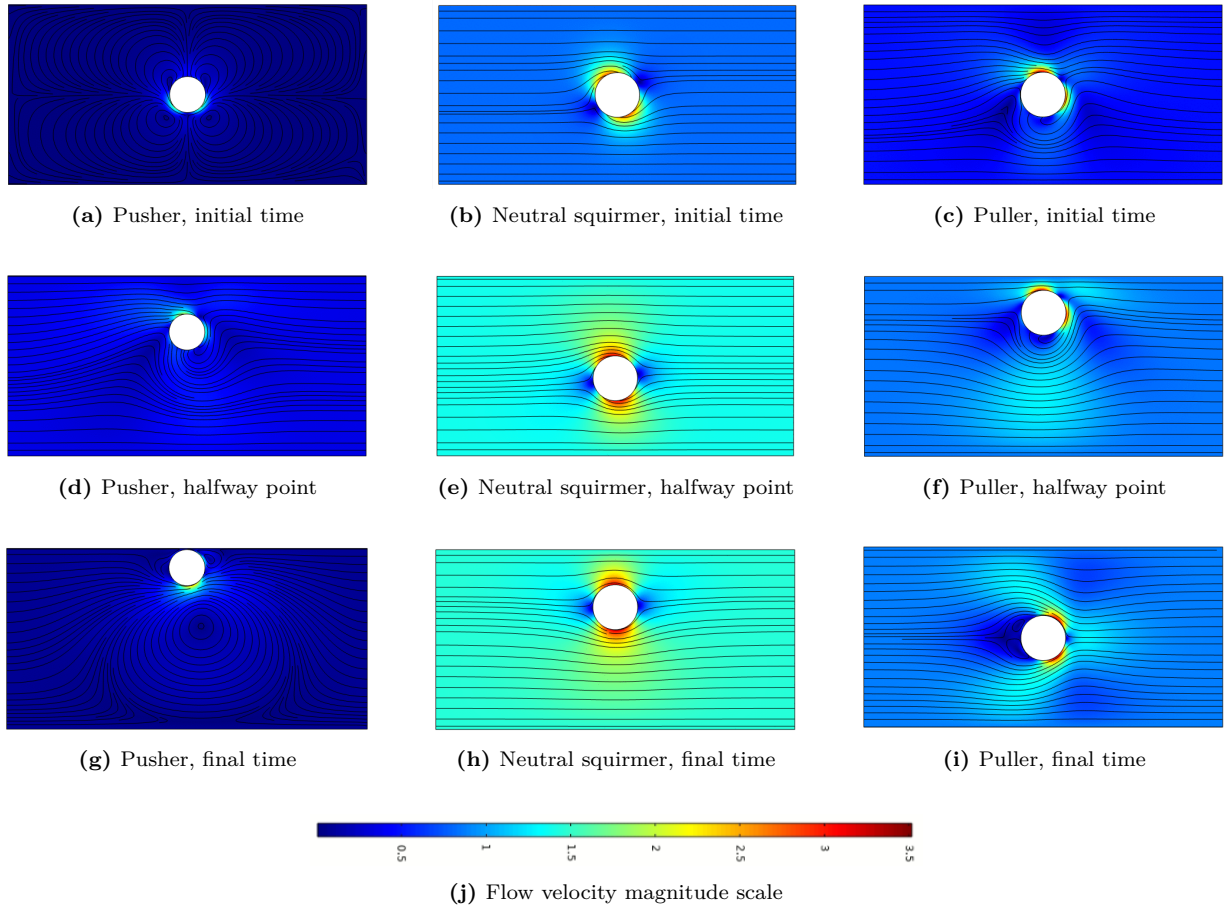


Figure 3.10: Figure showing the temporal evolution of velocity fields induced by a squirmer with first swimming mode $B_1 = 2$ in a rectangular microchannel. The figure displays velocity fields for different self-propulsion strengths (β), categorized as pusher ($\beta = -2$ in (a), (d), (g)), neutral squirmer ($\beta = 0$ in (b), (e), (h)), and puller ($\beta = 2$ in (c), (f), (i)). The black-coloured streamlines in each figure provide insights into propulsion mechanisms and highlight significant variations over time. The reference flow velocity magnitude scale is represented by (j).

Chapter 4

Appendix

The links provided below allow access to the source files for the MATLAB and COMSOL simulations, as well as the datasets related to squirmer dynamics:

- [Swimming dynamics in an infinite domain studied in the lab frame.](#)
- [Swimming dynamics in an infinite domain studied in the co-moving frame.](#)
- [Swimming dynamics in a confined domain studied in the lab frame.](#)
- [Swimming dynamics in a confined domain studied in the \$x\$ -moving frame.](#)

These links provide access to the necessary files to reproduce the simulations and analyze the results presented in this study.

References

- [1] Donald L Koch and Ganesh Subramanian. Collective hydrodynamics of swimming microorganisms: living fluids. *Annual Review of Fluid Mechanics*, 43:637–659, 2011.
- [2] Jens Elgeti, Roland G Winkler, and Gerhard Gompper. Physics of microswimmers—single particle motion and collective behavior: a review. *Reports on progress in physics*, 78(5):056601, 2015.
- [3] Saverio E Spagnolie and Eric Lauga. Hydrodynamics of self-propulsion near a boundary: predictions and accuracy of far-field approximations. *Journal of Fluid Mechanics*, 700:105–147, 2012.
- [4] Ye Li, He Zhai, Sandra Sanchez, Daniel B Kearns, and Yilin Wu. Noncontact cohesive swimming of bacteria in two-dimensional liquid films. *Physical review letters*, 119(1):018101, 2017.
- [5] Henry Shum and Eamonn A Gaffney. Hydrodynamic analysis of flagellated bacteria swimming near one and between two no-slip plane boundaries. *Physical Review E*, 91(3):033012, 2015.
- [6] Jeffrey A Riffell and Richard K Zimmer. Sex and flow: the consequences of fluid shear for sperm–egg interactions. *Journal of Experimental Biology*, 210(20):3644–3660, 2007.
- [7] Stefano Fusco, George Chatzipirpiridis, Kartik M Sivaraman, Olgaç Ergeneman, Bradley J Nelson, and Salvador Pané. Chitosan electrodeposition for microrobotic drug delivery. *Advanced healthcare materials*, 2(7):1037–1044, 2013.
- [8] Nicholas G Chisholm, Dominique Legendre, Eric Lauga, and Aditya S Khair. A squirmmer across reynolds numbers. *Journal of Fluid Mechanics*, 796:233–256, 2016.
- [9] P Ahana and Sumesh P Thampi. Confinement induced trajectory of a squirmmer in a two dimensional channel. *Fluid Dynamics Research*, 51(6):065504, 2019.

- [10] Deming Nie, Yuxiang Ying, Geng Guan, Jianzhong Lin, and Zhenyu Ouyang. Two-dimensional study on the motion and interactions of squirmers under gravity in a vertical channel. *Journal of Fluid Mechanics*, 960:A31, 2023.
- [11] Michael J Lighthill. On the squirming motion of nearly spherical deformable bodies through liquids at very small reynolds numbers. *Communications on pure and applied mathematics*, 5(2):109–118, 1952.
- [12] JR Blake. Self propulsion due to oscillations on the surface of a cylinder at low reynolds number. *Bulletin of the Australian Mathematical Society*, 5(2):255–264, 1971.
- [13] On Shun Pak and Eric Lauga. Generalized squirming motion of a sphere. *Journal of Engineering Mathematics*, 88:1–28, 2014.
- [14] Ingo O Götze and Gerhard Gompper. Mesoscale simulations of hydrodynamic squirmer interactions. *Physical Review E*, 82(4):041921, 2010.
- [15] G J Li, Alireza Karimi, and Arezoo M Ardekani. Effect of solid boundaries on swimming dynamics of microorganisms in a viscoelastic fluid. *Rheologica acta*, 53:911–926, 2014.
- [16] Nicholas C Darnton, Linda Turner, Svetlana Rojevsky, and Howard C Berg. Dynamics of bacterial swarming. *Biophysical journal*, 98(10):2082–2090, 2010.
- [17] Eric Lauga, Willow R DiLuzio, George M Whitesides, and Howard A Stone. Swimming in circles: motion of bacteria near solid boundaries. *Biophysical journal*, 90(2):400–412, 2006.
- [18] Federico Fadda, John Jairo Molina, and Ryoichi Yamamoto. Dynamics of a chiral swimmer sedimenting on a flat plate. *Physical Review E*, 101(5):052608, 2020.
- [19] Philip M Gresho, Robert L Lee, Robert L Sani, and TW Stullich. Time-dependent fem solution of the incompressible navier–stokes equations in two-and three-dimensions. Technical report, California Univ., 1978.
- [20] Roland Glowinski and Olivier Pironneau. Finite element methods for navier-stokes equations. *Annual review of fluid mechanics*, 24(1):167–204, 1992.
- [21] Cornelis Cuvelier, August Segal, and Anton A Van Steenhoven. *Finite element methods and Navier-Stokes equations*, volume 22. Springer Science & Business Media, 1986.

- [22] Kenta Ishimoto and Darren G Crowdy. Dynamics of a treadmilling microswimmer near a no-slip wall in simple shear. *Journal of Fluid Mechanics*, 821:647–667, 2017.
- [23] John F Brady and Georges Bossis. The rheology of concentrated suspensions of spheres in simple shear flow by numerical simulation. *Journal of Fluid Mechanics*, 155:105–129, 1985.
- [24] Takuji Ishikawa and TJ Pedley. Diffusion of swimming model micro-organisms in a semi-dilute suspension. *Journal of Fluid Mechanics*, 588:437–462, 2007.
- [25] Josephine Ainley, Sandra Durkin, Rafael Embid, Priya Boindala, and Ricardo Cortez. The method of images for regularized stokeslets. *Journal of Computational Physics*, 227(9):4600–4616, 2008.
- [26] Albert T Poortinga, Rolf Bos, Willem Norde, and Henk J Busscher. Electric double layer interactions in bacterial adhesion to surfaces. *Surface science reports*, 47(1):1–32, 2002.
- [27] Lailai Zhu, Eric Lauga, and Luca Brandt. Low-reynolds-number swimming in a capillary tube. *Journal of Fluid Mechanics*, 726:285–311, 2013.
- [28] Kai Qi, Hemalatha Annepu, Gerhard Gompper, and Roland G Winkler. Rheotaxis of spheroidal squirmers in microchannel flow: Interplay of shape, hydrodynamics, active stress, and thermal fluctuations. *Physical Review Research*, 2(3):033275, 2020.
- [29] Akash Choudhary, KVS Chaithanya, Sébastien Michelin, and S Pushpavanam. Self-propulsion in 2d confinement: phoretic and hydrodynamic interactions. *The European Physical Journal E*, 44:1–21, 2021.
- [30] Kevin J Anderson, Adelaide de Guillebon, Andrew D Hughes, Weiwei Wang, and Michael R King. Effect of circulating tumor cell aggregate configuration on hemodynamic transport and wall contact. *Mathematical biosciences*, 294:181–194, 2017.